Applied Catalysis B: Environmental 305 (2022) 121016

Contents lists available at ScienceDirect

Applied Catalysis B: Environmental

journal homepage: www.elsevier.com/locate/apcatb

Mechanism and sites requirement for CO hydrogenation to CH_3OH over Cu/CeO_2 catalysts

Pengchao Ren [a,1], Weifeng Tu [a,1], Chanchan Wang [a], Sifan Cheng [a], Wenqi Liu [a], Zhenzhou Zhang [a], Yun Tian [a], Yi-Fan Han [a,b,*]

[a] Engineering Research Center of Advanced Functional Material Manufacturing of Ministry of Education, Zhengzhou University, Zhengzhou 450001, China
[b] State Key Laboratory of Chemical Engineering, East China University of Science and Technology, Shanghai 200237, China

ARTICLE INFO

Keywords:
Syngas
Methanol synthesis
Cu-CeO_2 synergy
Interface
Active sites
Surface reactive intermediates

ABSTRACT

This study investigated the Cu-CeO_2 interactions for CO hydrogenation to methanol by applying rate measurements, chemical titration/desorption, together with in-situ/operando spectroscopy techniques under realistic reaction conditions. Ce components were enriched in the surface region of Cu/CeO_2 catalysts while Ce^{3+} and Ce^{4+} atoms co-existed during CO hydrogenation. The ratio of Ce^{3+} to Cu^0 in the surface region of catalysts increased linearly with the Ce content. The turnover rates of CH_3OH formation increased as a single-valued function of the ratio, irrespective to the individual contact extent between Cu and CeO_2 clusters or Ce content in the Cu/CeO_2 catalysts, indicating that the Cu^0-Ce^{3+} sites pair acts as active sites for CO hydrogenation to methanol over Ce-CeO_2 samples. This study also unraveled that formyl and formate species, as reactive surface intermediates, were co-adsorbed on the Cu^0-Ce^{3+} sites, and their hydrogenation routes occurred concurrently for CH_3OH formation during CO-H_2 reactions.

1. Introduction

Methanol is a building block for chemical industry and energy carrier, with a worldwide demand of ~100 million tons per year, which can either be used directly or further transformed to produce a wide range of chemicals (e.g. formaldehyde, olefins, methyl tert-butyl ether, or dimethyl ether) that ultimately find applications in diverse sectors (construction, textiles, packaging, furniture, paints, coatings, etc.). Methanol can be manufactured from a variety of sources, such as biomass, municipal waste, natural gas and coal, predominantly industrially synthesized from fossil-fuel based syngas (CO and H_2) with small amounts of CO_2 (< 5 vol%) over commercial $Cu/ZnO/Al_2O_3$ catalysts at pressures between 5 and 10 MPa and temperatures between 473 and 573 K. Both CO hydrogenation and CO_2 hydrogenation could occur concurrently during CO-CO_2-H_2 reactions, and the predominant reaction depends on the operating conditions (e.g. CO_2/CO ratios, temperature) [1,2]. Radiotracer experiments have shown that CO_2 rather than CO hydrogenation is the main synthesis route for methanol during CO-CO_2-H_2 reactions [1,2].

It is well known that methanol synthesis from CO_2 hydrogenation is a structure sensitive reaction over metal nanoparticles supported on oxides (Cu/Al_2O_3 [3], $Cu/ZnO/Al_2O_3$ [4], Cu/ZnO [5], Cu/CeO_2 [6,7], Pd/CeO_2 [8], or Au/ZnO [9]) and the inverse oxide clusters supported on metals (ZrO_2/Cu [10], ZnO/Cu(111) [11], or CeO_2/Cu(111) [12]). In general, a bare copper metal surface is widely regarded as the primary active phase in the forward, the reverse water-gas shift and in methanol synthesis. Oxides act as a physical spacer between the metal nanoparticles and stabilize the dispersion of metal clusters [13], but the synergistic effects between metal and oxide are thought to be responsible for the catalytic activity of these catalysts for methanol synthesis [5,14]. On the typical binary Cu/ZnO catalysts, the ionized oxygen vacancies on ZnO promoted by metallic Cu [15], the interfacial site of Cu-ZnO [5,14], Cu-metallic Zn [5] or defective Cu surface with a nearby Zn site [4] has been proposed as Cu-ZnO synergy to reflect the active sites for CO_2 hydrogenation. Meanwhile, the reducible oxide clusters (In_2O_3 [16–18], ZnO [11,19], CeO_2 [7,20,21], or Ga_2O_3 [22]) or mixed oxides (ZnO-Al_2O_3 [23], ZnO-ZrO_2 [24], or In_2O_3-ZrO_2 [25]) were recently attracted considerable attention for methanol synthesis. Oxides

* Corresponding author at: Engineering Research Center of Advanced Functional Material Manufacturing of Ministry of Education, Zhengzhou University, Zhengzhou 450001, China.
E-mail address: yifanhan@ecust.edu.cn (Y.-F. Han).
[1] Pengchao Ren and Weifeng Tu contribute equally to this work.

https://doi.org/10.1016/j.apcatb.2021.121016
Received 18 September 2021; Received in revised form 26 November 2021; Accepted 13 December 2021
Available online 16 December 2021

create oxygen vacancy sites for CO_2 activation and hydrogenation by stabilizing surface reactive intermediates (HCOO*, H_2COO*, or H_2CO*) [17,18], and their ability depends on their basicity and reducibility [26].

The active site for CH_3OH synthesis was found previously to depend on the composition of reactants. Early studies postulated that active sites for CO hydrogenation is Cu-O-Zn (or Cu-ZnO) while that for CO_2 hydrogenation is Cu-Zn^0 from the chemical state of Zn/Cu(111) surface by post-reaction surface analysis using XPS [27,28] or reduction-oxidation treatment of Cu/ZnO catalysts [29,30]. However, Kurtz et al. proposed that CO is adsorbed and activated at oxygen vacancies on ZnO surface which are blocked when CO_2 is added to the reactants [31]. Despite great efforts attempting to unravel the nature of the active sites for both CO_2 hydrogenation and CO hydrogenation to methanol have led to more debates and were not comprehensively understood due to the complexity of catalysts and lack of solid experimental evidence. Generally, the electronic and chemical states, geometric structures of catalysts are known to depend on the environment (temperature and gas composition) encountered during catalysis. The structure and composition of the synthesized or pretreated materials, especially for the bimetallic nanoparticles, change dynamically during catalysis. Therefore, characterizations of catalysts carried out offline could not determine the real active sites of catalysts and thus often corrupt the mechanistic interpretation of CO hydrogenation to methanol. Furthermore, previous studies revealed the potential of CuO/CeO_2 catalysts in methanol synthesis from CO hydrogenation and found that CuO/CeO_2 catalysts are more active in CO hydrogenation than conventional Cu/ZnO catalysts at lower temperature (< 473 K) [32,33]. The superior reactivity of Cu/CeO_2 catalysts was principally correlated with a synergistic effect linked to Cu-Ce interaction (either geometric or electronic) [34], however, the identity of the active sites on the Cu-CeO_2 catalysts at working state has not yet to be established for CO hydrogenation.

Density functional theory (DFT) calculations and experimental evidences indicate that CH_3OH formation from CO_2 hydrogenation is most probably via the formate route, which is eventually hydrogenated to methanol via the C-O bond cleavage in H_2COOH, with the hydrogenation of the formate (HCOO*) to HCOOH* as the rate-determining step [8,35–38]. However, the addition of CeO_2 nanoparticles to Cu(111) alters the relative stability of surface species of carboxylate (CO_2*) and HCOO*, thus the lower stability of the CO_2* species makes for a better intermediate for CH_3OH synthesis from CO_2 hydrogenation rather than the HCOO* species [7,12]. Similarly, mechanistic investigations using combined DFT calculation, kinetic Monte Carlo (KMC) simulations and diffuse reflectance IR Fourier transform spectroscopy (DRIFTS) showed that methanol synthesis from CO_2 hydrogenation on both TiO_2 and ZrO_2 supported Cu occurs via carboxyl intermediates while the formate species likely act as a spectator [39]. For CO hydrogenation to CH_3OH, basic oxide sites activate CO via formyl intermediate at the metal-oxide interface of Cu-CeO_2 [21] or formate species on Cu-MgO interface [40] followed by metal assisted hydrogenation of these surface intermediates. The interfacial sites are strongly inhibited by CO_2 due to the formation of carbonate species and thereby prevent the synergistic pathway from CO [21,40]. Therefore, the reactive surface intermediates and the routes of methanol synthesis strongly depend on the identities of the oxides and metal-oxide interface. Although many studies have been carried out to study the reaction mechanism of methanol synthesis, the reaction pathways and reactive surface intermediates over metal-oxide catalysts, especially for CO hydrogenation, still remain less explored.

In this study, we systematically tuned the Cu-CeO_2 interactions by altering the contact extent between Cu clusters and CeO_2 clusters and the atomic ratio of Cu to Ce to investigate in detail the role of the Cu-CeO_2 interactions for CO hydrogenation to CH_3OH. A combined approach of the steady-state intrinsic rate measurement, in-situ X-ray photoelectron spectroscopy (in-situ XPS), in-situ diffuse reflectance infrared Fourier transform spectroscopy (in-situ DRIFTS), chemical reactive titration, and temperature-programmed desorption of H_2 (H_2-TPD), was developed to identify the active sites and reaction pathway for CO hydrogenation to CH_3OH. We demonstrated that the Cu^0-Ce^{3+} sites pair represents the active sites at Cu-CeO_2 interface for CO hydrogenation. In particular, methanol was the dominant carbon containing product with carbon selectivity of above 97% during CO hydrogenation on Cu-CeO_2 catalysts, its formation rate (per exposed metallic Cu atom) increased linearly with the content of Ce in these Cu-CeO_2 catalysts. Tuning the Ce content did not vary the rate dependence for CH_3OH formation, and thus could not modify their reaction pathways and kinetically relevant steps. The atomic ratio of Ce^{3+} to Cu^0 in the surface layer of Cu/CeO_2 catalysts increased linearly with increasing Ce content, which adequately correlated with the trend of the reactivity of methanol formation. The results of H_2 uptakes and H_2-TPD also indicated that the surface Ce^{3+} atoms at the interface of Cu-CeO_2 increase linearly with the Ce content. Formyl and formate species were the reactive surface intermediates at Cu-CeO_2 interface and concurrently hydrogenated to form CH_3OH during CO-H_2 reactions.

2. Experimental methods

2.1. Preparation of Cu-CeO_2 samples

A series of Cu/CeO_2 catalysts with different Ce contents (mole fraction of Ce, Ce/(Ce+Cu) = 0.09, 0.17, 0.33, 0.40, 0.50 or 0.67) were prepared by a coprecipitation method. Stoichiometric quantities of $Cu(NO_3)_2$ (Macklin, 99.7% trace metals basis) and $Ce(NO_3)_3{\cdot}6H_2O$ (Aladdin, 99.5% trace metals basis) were dissolved in doubly deionized water (> 18.2 MΩ) under constant stirring at 353 K. An aqueous solution of KOH (0.1 M, KOH, Greagent, 99.8%) was added dropwise to the aqueous solution of $Cu(NO_3)_2$ and $Ce(NO_3)_3$ with constant stirring at 353 K until the pH value reached 10 ± 0.5. The mixed solution was kept at 353 K for 1 h and then cooled to ambient temperature. Precipitates were filtered (Taitan brand filter paper, coarse porosity, particle retention > 20 μm) and washed thoroughly with doubly deionized water (> 18.2 MΩ) until K^+ ions were no longer detected in the eluted water by using ICP (K^+ < 1 ppm). The resulted solids were dried at 373 K in ambient air for 12 h and then heat treated in flowing dry air at 723 K (a ramp rate of 0.017 $K{\cdot}s^{-1}$) for 4 h. The solids were pressed, grinded and sieved to retain 125–180 μm particles. The pure CuO and CeO_2 were prepared by coprecipitation method same as Cu/CeO_2.

Cu+CeO_2 agglomerates were prepared by physically mixing CuO powders (0–5 μm particle size) and CeO_2 powders (0–5 μm particle size) at CeO_2-to-Cu+CeO_2 atomic ratios between 0.09 and 0.50. Then the mixtures were subsequently pressed into pellets and sieved to retain 125–180 μm agglomerates.

2.2. Characterization of catalysts

The composition of the as-synthesized CuO/CeO_2 catalysts were determined by ICP-OES (Shimadzu ICPE-9820). Before measurements, the samples were dissolved in aqua regia at 313 K for 12 h.

Crystalline phases of the Cu-CeO_2 samples (Cu/CeO_2 catalysts and Cu+CeO_2 agglomerates) were identified on X-ray powder diffractometer (Bruker D8 Advance) using Cu Kα radiation as X-ray source (λ = 1.5418 Å) operating at 40 kV and 40 mA with the 2θ range from 10 to 80° at a scan rate of 0.033° s^{-1}. The XRD patterns of the reduced Cu-CeO_2 samples were collected after reduction under a flow of 5% H_2/Ar (0.5 $cm^3{\cdot}s^{-1}$) at an atmospheric pressure at 503 K for 1 h (heating rate of 0.083 K s^{-1}). After H_2 reduction, the samples were cooled under an Ar flow (0.5 $cm^3{\cdot}s^{-1}$) to 493 K, followed by exposure to CO-H_2 at 493 K for 3 h to collect the XRD patterns. The XRD patterns of the as-synthesized CuO-CeO_2 samples were obtained before H_2 reduction. The average crystalline sizes of Cu and CeO_2 in samples were calculated via the Scherrer equation [Eq. (1)] by the width of diffraction patterns with reference to the full width of half maximum of the crystalline facets at 35.4° for CuO (111) and 28.4° for CeO_2 (111) as follow:

$$D(\text{Å}) = \frac{k \times \lambda}{\beta(2\theta) \times \cos\theta} \quad (1)$$

Where D is the crystalline size (Å), k is the Scherrer constant (0.94), λ is X-Ray wavelength (Å), $\beta(2\theta)$ is full width of half maximum of the crystalline facets in radians.

Laser Raman spectra of CuO/CeO_2 samples were collected on a confocal Raman (LabRam HR Evolution, Horiba), which equipped with a high-grade Leica microscope (long working distance objective 50×) and a visible 532 nm laser. A spectral resolution of less than 0.5 cm^{-1} was achieved by using a 1200 lines/mm grating. The Raman shift was calibrated by interpolation of the Rayleigh line and a silicon wafer signal (520 cm^{-1}).

TEM images of the as-synthesized and spent Cu-CeO_2 samples were performed on a FEI TalosF200S transmission electron microscope (an acceleration voltage of 200 kV, cold field emission gun), equipped with an annular dark-field (ADF) detector and an energy-dispersive X-ray spectroscopy. The samples were dispersed onto a holey-carbon film supported on 300 mesh Cu TEM grid (Bhaddaji-tech (Beijing) Co., Ltd.). The analysis of the transmission electron microscopy (TEM) imaging and nanoparticle size of the catalysts was performed by using Gatan Digital Micrograph software (Version 3.9).

H_2-TPR and H_2-TPD measurements were performed using a custom-built micro-catalytic plug flow reactor (ID = 5.0 mm) system equipped with an online quadrupole mass spectrometry (Hiden analytical, HPR-20). The as-synthesized CuO/CeO_2 catalysts (180–250 μm, 100 mg) were held between plugs of quartz wool (Shanghai Xinhu Laboratory Equipment Co., Ltd., 4–10 μm) into the quartz plug flow reactor, and then treated in flowing Ar (Jining Xieli Special Gas Co., Ltd., 99.999%, flow rate 10 $cm^3 \cdot g_{cat}^{-1} \cdot s^{-1}$) at 673 K (a ramping rate of 0.17 $K \cdot s^{-1}$) for 1 h to remove water and surface hydroxyl species followed by cooling to 323 K in Ar (10 $cm^3 \cdot g_{cat}^{-1} \cdot s^{-1}$). The Ar-treated CuO/CeO_2 catalysts were heated at 0.17 $K \cdot s^{-1}$ from 323 K to 673 K in flowing 5% H_2/Ar (Jining Xieli Special Gas Co., Ltd, 99.999%, flow rate 5 $cm^3 \cdot g_{cat}^{-1} \cdot s^{-1}$) to obtain the profile of H_2-TPR. Next, the as-synthesized CuO/CeO_2 catalysts (125–180 μm, 100 mg) were initially treated at 503 K (a ramping rate of 0.083 $K \cdot s^{-1}$) under flowing 5% H_2/Ar (5 $cm^3 \cdot g_{cat}^{-1} \cdot s^{-1}$) for 3 h and then cooled to 493 K in flowing Ar (10 $cm^3 \cdot g_{cat}^{-1} \cdot s^{-1}$) before exposure to a flowing mixture (10 $cm^3 \cdot g_{cat}^{-1} \cdot s^{-1}$) of H_2 (Jining Xieli Special Gas Co., Ltd, 99.999%) and CO (Jining Xieli Special Gas Co., Ltd, 99.999%) at 493 K for 3 h. The pretreated catalysts were purged under an Ar flow of 10 $cm^3 \cdot g_{cat}^{-1} \cdot s^{-1}$ at 493 K for 5 h to remove all gaseous and surface adsorbed species derived from the CO-H_2 mixture and then cooled to 313 K in Ar (10 $cm^3 \cdot g_{cat}^{-1} \cdot s^{-1}$) for H_2 adsorption. H_2 adsorptions were carried out under a H_2 flow (5 $cm^3 \cdot g_{cat}^{-1} \cdot s^{-1}$) at 313 K for 0.5 h followed by purging in Ar (10 $cm^3 \cdot g_{cat}^{-1} \cdot s^{-1}$) at 313 K for 1 h to remove all gaseous H_2 and physically adsorbed H_2. H_2-TPD experiments of the treated catalysts were measured in Ar (5 $cm^3 \cdot g_{cat}^{-1} \cdot s^{-1}$) by heating at 0.083 $K \cdot s^{-1}$ from 313 K to 653 K.

The number of exposed metallic Cu atoms on the reduced Cu-CeO_2 samples (Cu/CeO_2 catalysts and Cu+CeO_2 agglomerates) was quantified by a N_2O reactive frontal Chromatography (N_2O-RFC) [41] measured by a custom-built micro quartz reactor (ID = 5.0 mm) connected to an online quadrupole mass spectrometry (Hiden analytical, HPR-20). The samples (125–180 μm) were pretreated in 5% H_2/Ar flow (5 $cm^3 \cdot g_{cat}^{-1} \cdot s^{-1}$) at 503 K (a ramping rate of 0.083 $K \cdot s^{-1}$) for 3 h and then purged under an Ar flow (10 $cm^3 \cdot g_{cat}^{-1} \cdot s^{-1}$) for 0.5 h to remove gaseous H_2. A small amount of Ce^{4+} might be reduced to Ce^{3+} after exposure of Cu-CeO_2 into H_2 [41], it increased the oxygen uptake from N_2O as every two surface Ce^{3+} is expected to react with one N_2O molecule ($Ce_2O_3 + N_2O = N_2 + 2CeO_2$). Recently, CO_2, as a weaker oxophilic gas than N_2O, can re-oxidize the surface Ce^{3+} to Ce^{4+} on Cu-CeO_2, but did not change the chemical state of surface Cu atoms [21]. Therefore, the pre-reduced Cu-CeO_2 was exposed to a flow of 5% CO_2/Ar (Jining Xieli Special Gas Co., Ltd, 99.999%, 5 $cm^3 \cdot g_{cat}^{-1} \cdot s^{-1}$) at 313 K for 0.5 h followed by purging in Ar (10 $cm^3 \cdot g_{cat}^{-1} \cdot s^{-1}$) at 313 K, to eliminate the contribution of surface Ce^{3+} during N_2O-RFC. Finally, the treated Cu-CeO_2 catalysts were exposed to a flow of 1% N_2O/Ar (Jining Xieli Special Gas Co., Ltd, 99.999%, 3.3 $cm^3 \cdot g_{cat}^{-1} \cdot s^{-1}$) at 313 K. The metallic Cu surface atoms (per gram of catalyst, n_{Cu^0}, $mol \cdot g_{cat}^{-1}$) was estimated from the consumption of N_2O (n_{N_2O}, $mol \cdot g_{cat}^{-1}$) based on the stoichiometry of $n_{Cu^0}/n_{N_2O} = 2$.

Isothermal CO or H_2 uptakes on Cu-CeO_2 samples (Cu/CeO_2 catalysts and Cu+CeO_2 agglomerates) after exposure to a reaction mixture of H_2 and CO at 493 K, were measured using a custom-built chemisorption apparatus as described previously [42], at 313 K between 0 kPa and 13.0 kPa CO or H_2. The Cu-CeO_2 samples were first treated in 5% H_2/Ar (5 $cm^3 \cdot g_{cat}^{-1} \cdot s^{-1}$) at atmospheric pressure at 503 K for 3 h (a ramping rate of 0.083 $K \cdot s^{-1}$), then cooled to 493 K in Ar (10 $cm^3 \cdot g_{cat}^{-1} \cdot s^{-1}$) before exposure to a flow of CO-H_2 reaction mixture at atmospheric pressure and 493 K for 3 h. After the above treatments, the samples were exposed to dynamic vacuum ($< 9.0 \times 10^{-3}$ mPa) at 493 K for 5 h to completely remove all surface adsorbed species, and then cooled under dynamic vacuum to 313 K for CO or H_2 adsorption measurements. Two CO (or H_2) uptakes were collected consecutively, and the samples were evacuated under dynamic vacuum at 313 K for 0.5 h between these measurements. The irreversible CO (or H_2) uptakes were determined from the difference between the extrapolated values from the two isothermal uptakes to zero CO (or H_2) pressure.

The chemical state and the distribution of surface atomic composition of Cu/CeO_2 catalysts and Cu+CeO_2 agglomerates during methanol synthesis were measured with a near ambient-pressure X-ray photoelectron spectrometer (SPECS) equipped with a monochromatic Al Kα X-ray source ($h\nu$ = 1486.6 eV, operating at 15 kV and 80 W) and a high-pressure reactor. The Cu-CeO_2 samples were pressed onto a clean stainless-steel plate and then transferred into the high-pressure reactor. The Cu-CeO_2 samples were firstly reduced under 0.5 MPa of 5.0% H_2/Ar (5 $cm^3 \cdot g_{cat}^{-1} \cdot s^{-1}$) at 503 K (a ramping rate of 0.083 $K \cdot s^{-1}$) for 3 h, and then cooled to 493 K in Ar (10 $cm^3 \cdot g_{cat}^{-1} \cdot s^{-1}$) before exposure to a flowing mixture of H_2 and CO (10 $cm^3 \cdot g_{cat}^{-1} \cdot s^{-1}$, 0.5 MPa) at 493 K for 3 h. After the above treatment, Cu-CeO_2 samples were purged with Ar (10 $cm^3 \cdot g_{cat}^{-1} \cdot s^{-1}$) at 493 K for 5 h under an atmosphere pressure and subsequently exposed to dynamic vacuum before cooling to ambient temperature. The treated Cu-CeO_2 samples were transferred into the chamber under dynamic vacuum ($< 9.0 \times 10^{-4}$ Pa) for XPS analysis. The spectra were collected in CO-H_2 mixture (60 Pa H_2 and 5 Pa CO) at 493 K with a total pressure of 100 Pa (step of 0.05 eV and pass energy of 25 eV), and deconvoluted using a Casa XPS software with all electron binding energies (BE) referred to the peak of C1s at 284.6 eV.

Operando Diffuse Reflectance Infrared Fourier Transform spectroscopy (DRIFTS) studies on Cu/CeO_2 catalysts were performed on a thermo iS50 Fourier transform infrared spectrometer equipped with a mercury-cadmium-telluride (MCT) liquid-nitrogen-cooled detector and a reaction cell. The Cu/CeO_2 were reduced in 5% H_2/Ar (0.5 $cm^3 \cdot s^{-1}$) at an atmospheric pressure and 503 K for 3 h (a ramping rate of 0.083 $K \cdot s^{-1}$) in the reaction cell, and then cooled to 493 K in Ar (1 $cm^3 \cdot s^{-1}$). A background was taken before the exposure to CO-H_2 mixture (60 kPa H_2 and 5 kPa CO, 100 kPa total pressure) at 493 K. The operando infrared spectra were collected during methanol synthesis under the CO-H_2 mixture in the range of 1000–4000 cm^{-1} by averaging 64 scans with a resolution of 4 cm^{-1}. The products were analyzed by an on-line mass spectrometer. After exposure to CO-H_2 mixture at 493 K for 2.6 h, these Cu/CeO_2 catalysts were directly exposed either to 60% H_2/Ar (0.67 $cm^3 \cdot s^{-1}$) or Ar (0.67 $cm^3 \cdot s^{-1}$) at 493 K, to obtain the evolution of surface intermediate species. The intensity of IR vibration bands was normalized basing on the one collected after it reached steady-state during CO-H_2 reaction at 493 K.

CO-DRIFTS experiments were conducted after methanol synthesis in CO-H_2 mixture at 493 K. The Cu/CeO_2 catalysts were reduced in 5% H_2/Ar (0.5 $cm^3 \cdot s^{-1}$) at an atmospheric pressure and 503 K for 3 h (a ramping rate of 0.083 $K \cdot s^{-1}$) in the reaction cell, and cooled to 493 K in Ar (1 $cm^3 \cdot s^{-1}$). Then the samples were treated in CO-H_2 mixture (60 kPa

H_2 and 5 kPa CO, 100 kPa total pressure; 0.67 $cm^3 \cdot s^{-1}$) at 493 K for 3 h, followed by purging in Ar (1 $cm^3 \cdot s^{-1}$) at 493 K for 5 h to completely remove all gaseous species and surface adsorbed species, before cooling in Ar (1 $cm^3 \cdot s^{-1}$) to 313 K. The background of these samples was collected in Ar at 313 K. These samples were then exposed to 5% CO/Ar (0.67 $cm^3 \cdot s^{-1}$) at 313 K for 0.5 h, followed by purging in Ar flow (0.67 $cm^3 \cdot s^{-1}$) at 313 K. The infrared spectra for CO adsorption on the treated samples were collected at 313 K in Ar (0.67 $cm^3 \cdot s^{-1}$).

2.3. Steady-state catalytic rate

All Cu-CeO_2 samples (Cu/CeO_2 catalysts and $Cu+CeO_2$ agglomerates, 125–180 μm) were physically mixed with SiO_2 particles (Shanghai Titan Scientific Co., Ltd., 99.5%, 125–180 μm) to form a packed catalyst bed with a SiO_2-to-catalyst mass ratio of 1. The catalyst and SiO_2 mixtures were held between plugs of quartz wool in a quartz tubular micro catalytic plug flow reactor (5 mm reactor ID) contained within a stainless-steel reactor which equipped a K-tpye thermocouple (Omega, KMQXL-032G-12) placed in firm contact with the external wall of the stainless-steel reactor. Prior to the reaction, the samples were pretreated in 5% H_2/Ar (5 $cm^3 \cdot g_{cat}^{-1} \cdot s^{-1}$) at 503 K (a ramping rate of 0.083 $K \cdot s^{-1}$) for 3 h and then cooled to 493 K in Ar (10 $cm^3 \cdot g_{cat}^{-1} \cdot s^{-1}$) before exposure to CO-$H_2$ mixture. The reaction pressure was measured with an analog high-pressure transducer (MKS, Baratron absolute capacitance manometer, 750 C) installed at the inlet of the stainless-steel reactor, controlled by a back-pressure regulator (BRP, Tescom, 26–1765–22) located at the downstream of the reactor. All transfer gas lines downstream of the reactor were heated to 393 K to prevent the condensation of products. The chemical compositions of the reactants and products were quantified using an online gas chromatograph (Shanghai Ruimin Instrument Co., Ltd., GC2060) equipped with a HP-PLOT Q capillary column (Agilent, 19091P-Q04, 30 m × 320 μm × 20 μm) connected to a flame ionization detector (FID) and molecular sieve capillary column (TDX-01) connected to a thermal conductivity detector (TCD).

Rates of CH_3OH formation (r_{CH_3OH}, $mol \cdot g_{cat}^{-1} \cdot s^{-1}$) were measured in the kinetically controlled regime and at CO and H_2 conversions below 10%, taken after reaching steady-state, during which the errors in rates were less than 5% of their values for the entire duration of rate measurements (~100 h). The formation rate of CH_3OH [r_{CH_3OH}, Eq. (2)] and turnover rates of CH_3OH formation [TOF, Eq. (3), per mole of surface Cu^0 atom] were determined as following:

$$r_{CH_3OH}\left(mol \cdot g_{cat}^{-1} \cdot s^{-1}\right) = \frac{F \times n_{CH_3OH}}{m_{cat}} \quad (2)$$

$$TOF\left(s^{-1}\right) = \frac{r_{CH_3OH}}{n_{Cu^0}} \quad (3)$$

Where F is the flow rate of the gas mixture ($mol \cdot s^{-1}$) at the outlet of reactor, n_{CH_3OH} is the molar fraction of methanol (%), m_{cat} is the weight of catalyst (g), n_{Cu^0} refers the mole of surface metallic Cu atoms per gram of catalyst.

The conversion of CO was calculated by the difference in the molar flow rate of CO between the inlet and outlet of the reactor [Eq. (4)]:

$$X_{CO} = \frac{F_{CO,in} - F_{CO,out}}{F_{CO,in}} \times 100\% \quad (4)$$

Where $F_{CO,\ in}$ and $F_{CO,\ out}$ represent the molar flow rate of CO at the inlet and outlet of reactor, respectively. The carbon selectivity was calculated by molar flow rate of product j ($F_{j,out}$, j = CH_3OH, CO_2, or CH_4) per the molar flow rate of the converted CO [Eq. (5)]:

$$S_j = \frac{F_{j,out}}{F_{CO,in} - F_{CO,out}} \times 100\% \quad (5)$$

The water-gas-shift (WGS) reaction may occur concomitantly with CO-H_2 reaction, thus we defined an approach-to-equilibrium value (η_{WGS}) to determine the extent to which the WGS reaction deviates from chemical equilibrium during CO-H_2 reaction [Eq. (6)]:

$$\eta_{WGS} = \frac{P_{CO_2} P_{H_2}}{P_{CO} P_{H_2O}} \frac{1}{K_{WGS}} \quad (6)$$

Where P_i (i = CO, H_2O, CO_2, or H_2) is the partial pressure of CO, H_2O, CO_2, or H_2 at the outlet of reactor; the K_{WGS} denotes the chemical equilibrium constant for the WGS reaction.

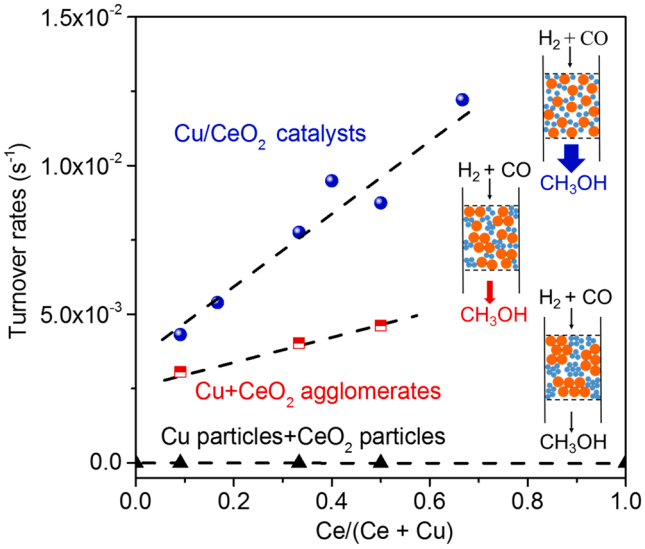

Fig. 1. Effects of Ce content and the extent (Cu/CeO_2 catalysts, $Cu+CeO_2$ agglomerates and mixture of Cu particles and CeO_2 particles) of Cu-CeO_2 interfaces on the turnover rates (TOF) of methanol formation from CO-H_2 at 493 K over Cu-CeO_2 samples (1030 kPa H_2, 75 kPa CO, 1500 kPa total pressure, GHSV of 18000 $cm^3 \cdot g_{cat}^{-1} \cdot h^{-1}$).

3. Results and discussion

3.1. Activity of methanol synthesis

Fig. 1 shows the turnover rates of methanol formation from CO-H_2 at 493 K over a series of Cu-CeO_2 samples. The conversion of CO and the formation rates of methanol were below the experimental detection limits (1 ppm of CH_3OH) during CO-H_2 reaction at 493 K over monometallic Cu, CeO_2, or the physically mixed Cu particles and CeO_2 particles (Ce to Ce+Cu atomic ratio of 0.09–0.50). The catalytic CO-H_2 reaction at 493 K on the Cu clusters supported on CeO_2 (Cu/CeO_2) yielded CH_3OH as a main carbon containing product. The turnover rates of CH_3OH formation over the series of Cu/CeO_2 catalysts remained independent of time (Fig. S2, ~100 h), with the conversion of CO less than 10% (Fig. S3a). The carbon selectivity toward CH_3OH formation exceeded 97% (Fig. S3b), with the carbon balance of above 95%. Moreover, the undetectable H_2O, probably formed via CO_2 hydrogenation for CH_3OH synthesis and/or reverse water-gas-shift reaction, together with the extremely low values (0.0 ± 0.1) of the approach-to-equilibrium value (η_{WGS}) for WGS reaction (Fig. S3d), indicates that both the RWGS reaction and CH_3OH from CO_2 hydrogenation did not occur at detectable rates during CO-H_2 reaction over these Cu-CeO_2 samples. CO-H_2 reactions did not form CH_4 at the detectable concentrations (detection limit of 1 ppmv) over Cu/CeO_2 catalysts at 493 K, thus the methanation must be negligible during CO hydrogenation. The CeO_2 might function as a physical spacer between Cu clusters and alter the cluster size of Cu or the exposed Cu facets, thus, modified the rates of the structural-sensitive methanol synthesis over Cu clusters [21,43]. Indeed, the turnover rates on different Cu facets, reported from single crystal studies, were extremely low as 1.3×10^{-6} to 6×10^{-3} s^{-1} per surface Cu atoms. However, the rates of CH_3OH formation (per surface

Table 1
Structure properties of the Cu/CeO_2 catalysts with different Ce contents (Ce/(Ce+Cu) = 0.09, 0.17, 0.33, 0.40, 0.50, and 0.67).

Ce/(Ce+Cu)	2θ (°) CeO_2(111)	Mean crystalline size (nm)						CuO/CeO_2 BET surface area ($m^2 \cdot g^{-1}$)
		As-synthesized		H_2 reduction		$CO-H_2$ reaction		
		CuO	CeO_2	Cu	CeO_2	Cu	CeO_2	
0.09	28.41	27.6	4.5	40.2	4.7	44.8	4.5	31.7
0.17	28.41	26.7	4.5	43.2	4.3	43.6	4.7	56.1
0.33	28.40	22.2	4.9	41.1	4.9	42.6	5.2	67.8
0.40	28.42	22.1	4.8	40.1	4.9	41.0	5.1	62.1
0.50	28.43	–	5.0	29.3	5.4	32.6	5.3	75.8
0.67	28.45	–	8.4	30.7	8.6	35.3	8.5	51.3

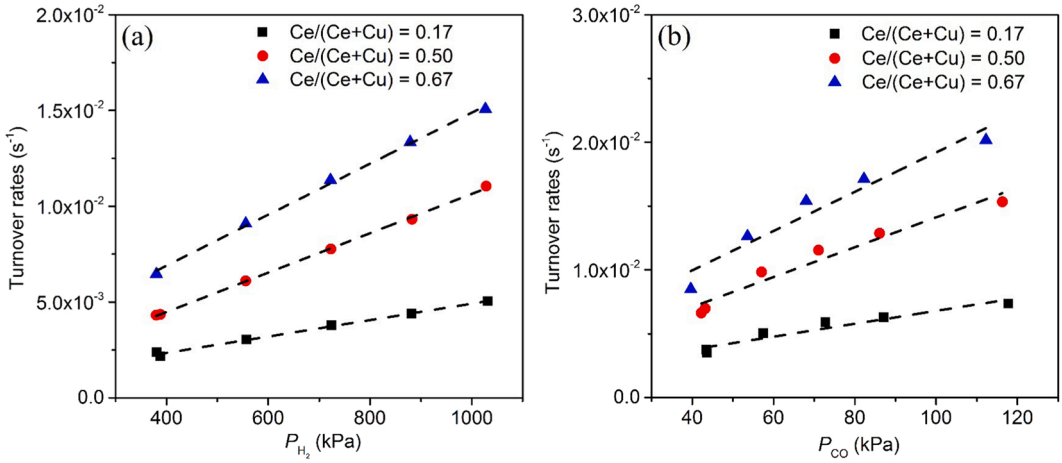

Fig. 2. Turnover rates of CH_3OH formation as function of (a) H_2 pressure (380–1030 kPa H_2, 80 kPa CO, 1500 total pressure; GHSV of 36000 $cm^3 \cdot g_{cat}^{-1} \cdot h^{-1}$, 493 K) and (b) CO pressure (40–120 kPa CO, 600 kPa H_2, 1500 total pressure, GHSV of 36000 $cm^3 \cdot g_{cat}^{-1} \cdot h^{-1}$, 493 K) during $CO-H_2$ reactions over Cu/CeO_2 catalysts with different Ce contents (Ce/(Ce+Ce) = 0.17, 0.50, and 0.67).

Cu atoms, determined by N_2O chemical titration, Fig. S1) were at least one order of magnitude higher than those on monometallic Cu facets, and increased linearly from 4.32×10^{-3} to 1.2×10^{-2} s^{-1}, in Fig. 1, with increasing the Ce content (9–67%) in the Cu/CeO_2 catalysts. These results agreed that surface Cu sites did not represent the active site for methanol synthesis [44]. The Cu clusters (29–43 nm Cu clusters, Table 1) in these Cu/CeO_2 catalysts were insensitive to the content of Ce, thus could not alter the formation rates of CH_3OH. A recent study proposed that the combination of metal and oxide centers in the Cu-Ce interfaces acts the active sites for methanol synthesis during CO_2 hydrogenation [7]. The Cu-Ce interfaces sites may also be the active sites during CO hydrogenation for CH_3OH formation. The presence of CeO_2 increases the activities of Cu clusters for CH_3OH synthesis, may due to the metal-oxide synergy or strong metal-support interaction (SMSI), reported previously during methanol synthesis from CO [20,21] or CO_2 [7,26,45]. The SMSI could modify the redox properties of both Cu and CeO_2 [26,46–48].

We next tuned the extent of the interaction between Cu clusters and

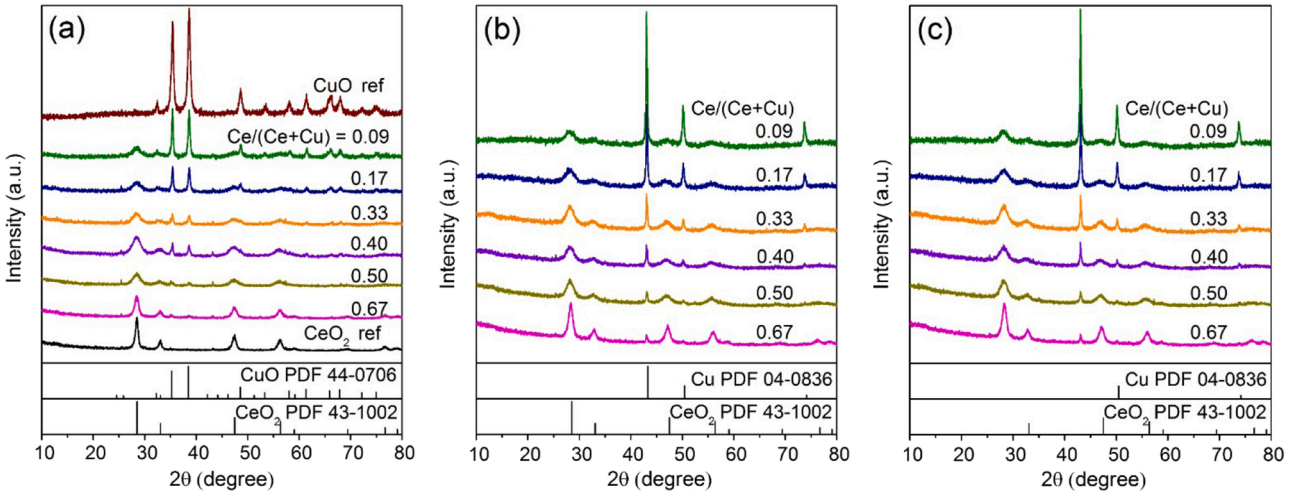

Fig. 3. XRD patterns of (a) the as-synthesized CuO/CeO_2, (b) H_2 (5 kPa H_2, 100 kPa total pressure, 503 K) and (c) $CO-H_2$ (60 kPa H_2, 5 kPa CO, 100 kPa total pressure, 493 K) treated Cu/CeO_2 catalysts with different Ce contents (Ce/(Ce+Ce) = 0.09, 0.17, 0.33, 0.40, 0.50, and 0.67).

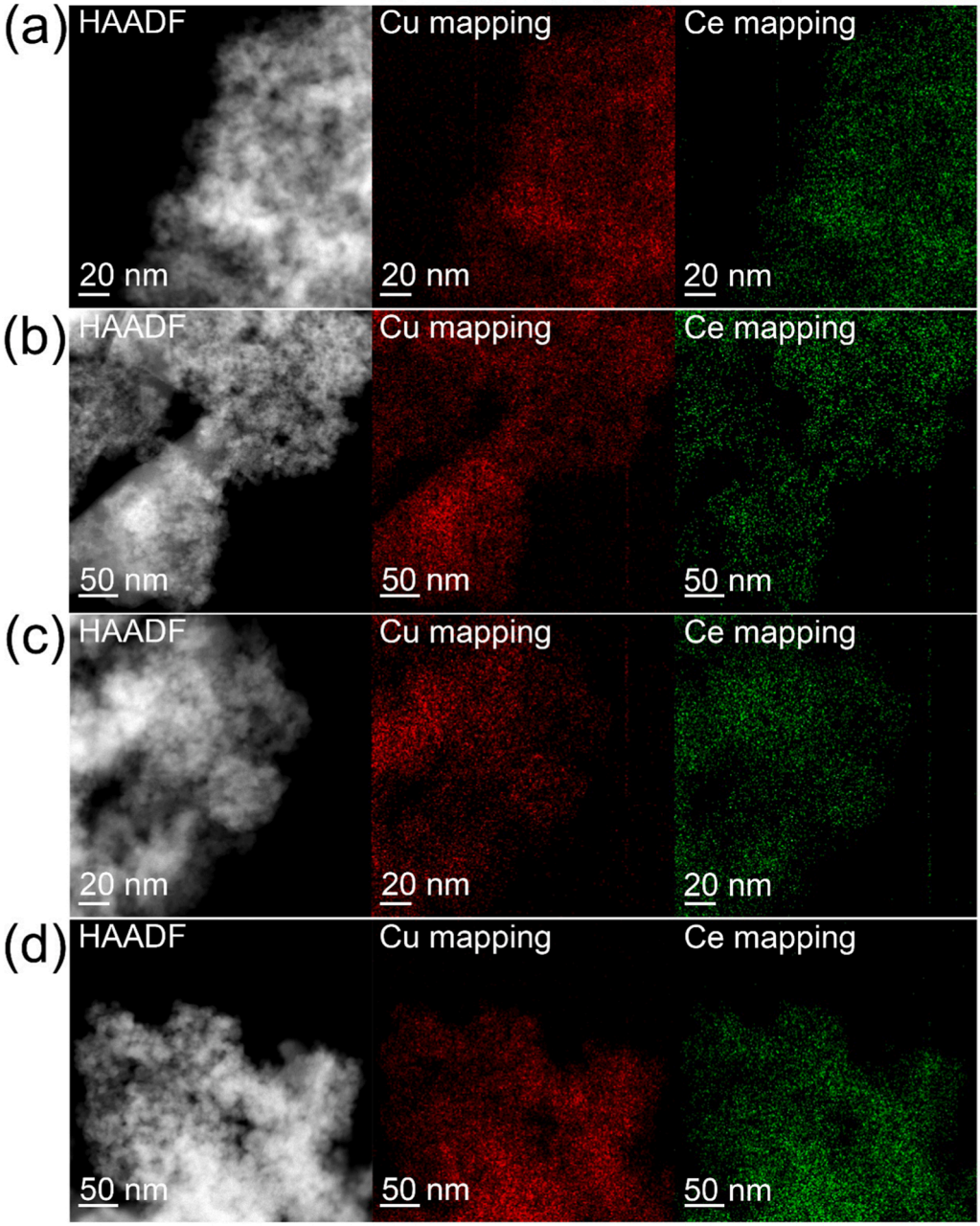

Fig. 4. HDAAF-STEM images with EDX elemental mapping of the as-synthesized CuO/CeO_2 with different Ce contents (Ce/(Ce+Ce) = 0.17 (a), 0.33 (b), 0.50 (c), and 0.67(d)).

CeO_2 clusters and their reactivity to probe the active sites of CH_3OH synthesis from CO-H_2, by physically mixing Cu clusters with CeO_2 clusters into agglomerates (125–180 μm) at CeO_2-to-Cu+CeO_2 agglomerate ratios between 0.09 and 0.50. On these Cu+CeO_2 agglomerates, CH_3OH was still the main carbon containing product (carbon selectivity > 97%). Although the formation rates of CH_3OH became much lower than those on the Cu/CeO_2 catalysts, but still significantly higher than those on the mixtures of Cu particles (70 ± 10 nm mean Cu cluster, 125–180 μm particles) and CeO_2 particles (9.0 ± 1.0 nm mean CeO_2 cluster, 125–180 μm particles). The CH_3OH formation rates still increased linearly from 3.06×10^{-3} to 4.62×10^{-3} s^{-1} at 493 K, with the content of CeO_2 in the Cu+CeO_2 agglomerates.

The identities and quantities of active sites, the catalytic steps, and their kinetic relevance are known to dictate the rates and selectivities during catalysis. The specific kinetically relevant steps and their rates usually vary with the identities on catalyst surfaces e.g, CH_4 oxidation on Pt/Al_2O_3 [49], Pd/Al_2O_3 [50], and bimetallic Pt-Pd/Al_2O_3 catalysts [51], dry reforming of CH_4 on Ni, Co, and Ni-Co clusters [52], or CH_3OH partial oxidation on Pt, Pd, Ag or Ru clusters [53]. Therefore, the difference in reactivities of CH_3OH synthesis over these Cu/CeO_2 catalysts might be caused by the variations in catalytic relevant steps during CO-H_2 reactions. We next probed the effects of the components of Cu/CeO_2 catalysts on the rate dependencies of CH_3OH formation during CO hydrogenation at 493 K. Fig. 2 shows the turnover rates of CH_3OH formation over a series of Cu/CeO_2 catalysts at 493 K as functions of reactants pressures. The formation rates of CH_3OH increased less than linearly with H_2 pressures (380–1030 kPa, 80 kPa CO) or CO pressures (40–120 kPa CO and 600 kPa H_2) at 493 K over Cu/CeO_2 catalysts. The apparent reaction orders with respect to CO and H_2 for CH_3OH formation were 0.80 ± 0.05 and 0.85 ± 0.05, respectively, and independent of the Ce content in Cu/CeO_2 catalysts (Fig. S4). Therefore, altering the ratio of Ce to Ce+Cu in Cu/CeO_2 catalysts did not influence the rate

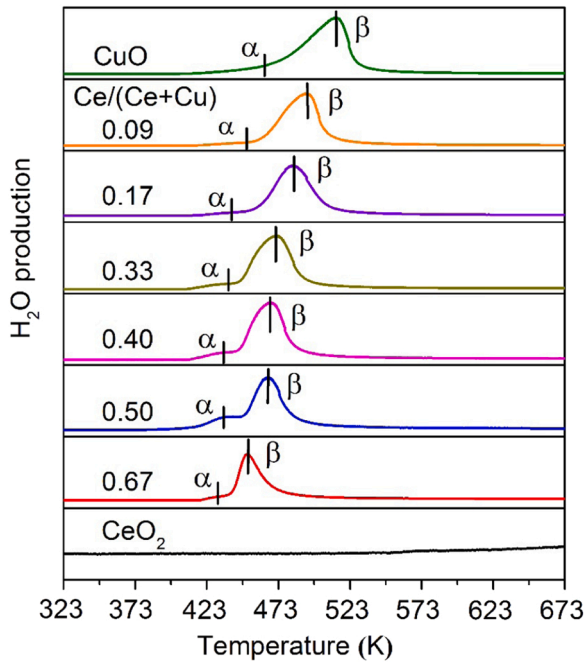

Fig. 5. H_2-TPR profiles of CuO, CeO_2 and as-synthesized CuO/CeO_2 catalysts with different Ce contents (Ce/(Ce+Ce) = 0.09, 0.17, 0.33, 0.40, 0.50, and 0.67) (5 kPa H_2, 100 kPa total pressure, 323–673 K).

dependences of CH_3OH synthesis from $CO-H_2$ reaction, could not alter the catalytic relevant steps for CH_3OH synthesis.

3.2. Effects of Ce content on the structure and texture of Cu/CeO_2 catalysts

Fig. 3 shows the X-ray diffraction (XRD) patterns of the as-synthesized, H_2 and $CO-H_2$ treated Cu/CeO_2 catalysts. The XRD patterns show the characteristic diffractions of the typical crystallized phases of CuO (PDF-# 44-0706, average crystalline size of 22–28 nm) and the fluorite-type structure of CeO_2 (PDF-# 43-1002, average crystalline size of 4.5–8.4 nm) [54–56] in the as-synthesized CuO/CeO_2. The intensity of CuO diffraction peaks deceased sharply with increasing the content of Ce from 0.0% to 50.0%, and then became undetectable with a further increase in Ce content. In contrast, the intensity of the crystalline phase of CeO_2 remained insensitive to the content of Ce in CuO/CeO_2 catalysts, while the diffraction peaks of CeO_2(111) slightly shifted to higher angles (2θ) with increasing Ce content (Table 1), indicating the formation of Cu-O-Ce solid solution in CuO/CeO_2 catalysts [56–59]. Cu-O-Ce solid solution was further determined by Raman spectra (Fig. S5). The peak of CeO_2 centered at 464 cm^{-1} was assigned to the F_{2g} vibrational mode [60], while the CuO exhibited the typical peaks at 284, 331 and 620 cm^{-1} attributed to A_g, B_{1g} and B_{2g} vibrational mode, respectively [56,61]. The characteristic F_{2g} peak of CeO_2 shifted gradually to lower wavenumber from 464 cm^{-1} to 452 cm^{-1} with increasing Ce content. The variation in Raman spectra suggests that the incorporation of Cu^{2+} into CeO_2 lattice led to the formation of the surface-substituted Cu-O-Ce solid solutions, and the creation of O vacancies compensated the charge discrepancy between Cu^{2+} and Ce^{4+} [41,56]. The Cu-O-Ce solid solutions might locate at the bottom layer of the CuO clusters or at the ceria surface as domains/monolayers, probably transforming to the interfacial copper species during H_2 reduction [41]. The morphological structure of the as-synthesized CuO/CeO_2 catalysts and $CuO+CeO_2$ agglomerates with different Ce contents were measured by transmission electron microscopy (TEM). High-resolution TEM (HR-TEM) images display the lattice spacing of CeO_2(111) and CeO_2(200) of 0.31 and 0.27 nm, respectively (Figs. S6 and S7), and the lattice spacing of 0.23 nm was assigned to CuO(111) (Fig. S7). The average particle size of CeO_2 nanoparticles in CuO/CeO_2 (4.8 ± 1.0 nm to 7.5 ± 1.0 nm, Fig. S6) was much smaller than that of CuO particles (20–40 nm), and partially covering the surface of CuO particles (Fig. S7). Energy-dispersive X-ray spectroscopy (EDX)-elemental mappings reveal a uniform distribution of CuO and CeO_2 clusters in the as-synthesized CuO/CeO_2 catalysts (Fig. 4). For $CuO+CeO_2$ agglomerates, a small part of surface of CuO particles with large particle size was covered by CeO_2 particles with small particle size, as shown in Fig. S8.

H_2 temperature-programmed reduction (H_2-TPR) was performed to explored the influence of Ce content on the reducibility of Cu/CeO_2 catalysts. The obtained H_2-TPR profiles are given in Fig. 5. The as-synthesized CuO/CeO_2 catalysts showed two distinct reduction peaks at temperature range of 420–520 K, which clearly illustrates distinct types of Cu species in CuO/CeO_2 [62,63]. The reduction peak (α) below 450 K was attributed to the reduction of the highly dispersed CuO clusters interacted weakly with CeO_2, while the strong reduction peak (β) above 450 K was assigned to the reduction of both Cu-O-Ce solid solution and surface CeO_2 species [34,41,64]. The H_2-TPR peaks of CuO/CeO_2 gradually shifted to lower temperatures (α peak: from 458 K to 429 K; β peak: from 513 K to 451 K; Table S1 and Fig. 5) with increasing the ratio of Ce/(Ce+Cu) from 0.0 to 0.67, indicating the reducibility of CuO strongly depended on the content of Ce. The promotion of CeO_2 on the reduction of CuO might be caused by the strong $Cu-CeO_2$ interaction [41].

After treated in H_2 at 503 K for 3 h, the CuO/CeO_2 catalysts became as a mixture of metallic Cu (Fig. 3b, average crystalline size of 29–43 nm, PDF-# 04-0836) and CeO_2 (Fig. 3b, average crystalline size of 4.3–8.5 nm, PDF-# 43-1002), which indicates that the CuO components were completely reduced and ultimately formed bulk metallic Cu particles while the CeO_2 remained its oxidative bulk. The HR-TEM images (Fig. S9) show that the reduced Cu/CeO_2 catalysts, after treated in $CO-H_2$ mixture at 493 K, remained as a mixture of metallic Cu (lattice spacing of 0.21 nm for Cu(111)) and CeO_2 (lattice spacing of 0.31 and 0.27 for CeO_2(111) and CeO_2(200), respectively), which agrees with the results of XRD in Fig. 3c. The CeO_2 particles with smaller size covered a large portion of the surface of Cu particles with bigger size, forming visible $Cu-CeO_2$ interfaces between Cu and CeO_2 particles (Fig. S9). In addition, the XRD patterns show the characteristic diffractions of the crystallized phases of CuO (PDF-# 44-0706, average crystalline size of 30 nm, Table S3) and CeO_2 (PDF-# 43-1002, average crystalline size of 10 nm; Table S3) in the as-synthesized $CuO+CeO_2$ agglomerates (Fig. S10a). After H_2 treatment, $Cu+CeO_2$ agglomerates exhibited the crystallized phases of both metallic Cu (70 ± 10 nm, Table S3 and Fig. S10b) and CeO_2 (9.0 ± 1.0 nm, Table S3 and Fig. S10b). The crystallized phase and cluster size of both Cu and CeO_2 in these $Cu+CeO_2$ agglomerates did not change after exposure to $CO-H_2$ mixture at 493 K for CH_3OH synthesis (Table S3 and Fig. S10c). Physically mixing Cu particles and CeO_2 particles in agglomerates (125–180 μm) did not alter the particle sizes of Cu (70 ± 10 nm, Table S3) and CeO_2 (9.0 ± 1.0 nm, Table S3).

3.3. Effects of Ce content on the chemical state of Cu/CeO_2 catalysts

The chemical state and the distribution of elements in surface region of $Cu-CeO_2$ samples were analyzed by *ex-situ*/in-situ ambient-pressure X-ray photoelectron spectroscopy (AP-XPS) under $CO-H_2$ mixture at 493 K. The XPS spectra show the Cu 2p, Cu LMM and Ce 3d region for the as-synthesized CuO/CeO_2 catalysts (Figs. S11 and S12). Spectra analysis revealed that the Cu 2p signals at 932.8 eV and their satellite signals at 942.0 eV were assigned to the Cu^{2+} species (Fig. S11a), this assignment was further confirmed by Cu auger peaks at 569.0 eV (Fig. S11b) [65]. Deconvolution of the Ce 3d spectra (Fig. S12) of the as-synthesized catalysts showed only one chemical state of Ce^{4+} species [12,66,67]. The surface atomic fractions of Ce (Ce/(Ce+Cu)), calculated from XPS spectrum, were higher than the bulk atomic fraction of Ce

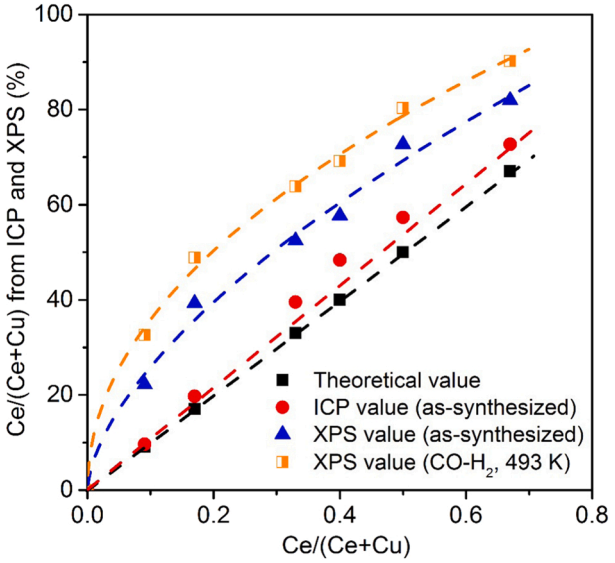

Fig. 6. Surface composition of the as-synthesized CuO/CeO_2 and Cu/CeO_2 catalysts during $CO\text{-}H_2$ reaction (60 Pa H_2 and 5 Pa CO) at 493 K, determined by ICP and *ex-situ*/in-situ XPS.

(measured by ICP) for all these CuO/CeO_2 catalysts with different Ce contents (Fig. 6), which confirms that the Ce species were enriched on the surface of the as-synthesized CuO/CeO_2. This is consistent with TEM results that highly dispersed CeO_2 clusters (4.5–8.4 nm) partially covered the CuO cluster surface (22–28 nm mean CuO cluster size) in these as-synthesized CuO/CeO_2 catalysts. After exposure of the Cu/CeO_2 catalysts into $CO\text{-}H_2$ mixture (493 K; 60 Pa H_2 and 5 Pa CO) at 493 K, the surface Ce/(Cu+Ce) ratios increased by 5.7–11.4% compared with those of as-synthesized CuO/CeO_2 catalysts (Fig. 6), suggesting that the Ce species prefer to migrate onto the catalyst surface during methanol synthesis.

The Cu 2p and Cu LMM XPS spectra were used to identify the valence state of Cu component in these Cu-CeO_2 samples during methanol synthesis. The binding energies (BE) of Cu 2p3/2 and Cu LMM maintained at 932.4 eV and 567.7 eV, respectively, for these Cu/CeO_2 catalysts (Figs. 7a and S13), $Cu+CeO_2$ agglomerates (Fig. S14), and monometallic Cu particles (Fig. S15). Deconvolution of these Cu 2p and Cu LMM spectra reveals that the Cu^+ and Cu^{2+} species were all negligible on these samples. These results indicate that the surface Cu species existed in a form of metallic Cu state during CH_3OH synthesis, irrespective to the content of Ce and the extent of Cu and Ce interactions in these Cu-CeO_2 samples (Cu/CeO_2 catalysts and $Cu+CeO_2$ agglomerates). Metallic Cu species were also reported previously as the dominant Cu species in Cu/ZnO [4,5] and Cu/ZrO_2 [68] catalysts.

Deconvolution of the Ce 3d spectra (Figs. 7b and S16) of the Cu-CeO_2 samples (Cu/CeO_2 catalysts and $Cu+CeO_2$ agglomerates), according to previously reported methodology [41,64,67,69,70], showed two chemical states of Ce species (Ce^{3+} and Ce^{4+}) coexisted in the surface layers of Cu-CeO_2 samples during methanol synthesis under $CO\text{-}H_2$ mixture at 493 K. The fraction of surface Ce^{3+} species was estimated by the ratio of the integration of Ce^{3+} peak areas to the integration of both Ce^{4+} and Ce^{3+} peak areas [41,67]. The fraction of Ce^{3+} was 14.7 ± 0.9% in the surface layers of the monometallic CeO_2 exposed to $CO\text{-}H_2$ mixture at 493 K (Fig. S17). However, the fraction of Ce^{3+} species was higher in the surface layers of Cu/CeO_2 catalysts than that of monometallic CeO_2, and increased significantly from 30.2 ± 1.1% to 67.2 ± 1.9% (Fig. S18a) with decreasing Ce content in these Cu/CeO_2 catalysts. More surface Ce^{3+} on Cu/CeO_2 catalysts with higher Cu-to-Ce ratio suggests that metallic Cu species facilitate the reduction of surface CeO_2 and formation of Ce^{3+} surface species. Previous DFT + U calculations reported that the charge transfer process occurred between metallic Cu and the adjacent Ce^{4+} species and resulted in the reduction of Ce^{4+} to Ce^{3+} [34,71]. Moreover, the reduction of Ce^{4+} to Ce^{3+} was observed in $CeO_x/Cu(111)$ model catalyst under H_2-rich CO_2 hydrogenation conditions [7]. It is clear that Ce^{3+} is more stable at Cu-Ce interface in comparison with Ce^{4+} [72], especially in strongly reducing atmosphere such as $CO\text{-}H_2$ mixture. Indeed, the fraction of surface Ce^{3+} was lower on these $Cu+CeO_2$ agglomerates than those on Cu/CeO_2 catalysts, but still higher than that of the monometallic CeO_2, which increased from 24.3 ± 1.0% to 38.1 ± 1.4% with decreasing Ce content in these $Cu+CeO_2$ agglomerates (Fig. S18a). Strong interaction between Cu and CeO_2 has been previously proposed on Cu/CeO_2 catalysts from XAFS [73] and H_2-TPR [41] studies. As results, both the extent of the interaction between Cu clusters and CeO_2 clusters and the ratio of Cu-to-Ce determine the surface fraction of Ce^{3+} in Cu/CeO_2 catalysts. The ratio of Ce^{3+} to Cu^0 (Ce^{3+}/Cu^0) in the surface layers of the Cu/CeO_2 catalysts during methanol synthesis, increased linearly from 0.32 to 2.33 with increasing Ce content (Fig. 8). These ratios in the $Cu+CeO_2$ agglomerates were smaller than those in Cu/CeO_2 catalysts, but still increased linearly from 0.10 to 0.28 with increasing Ce content.

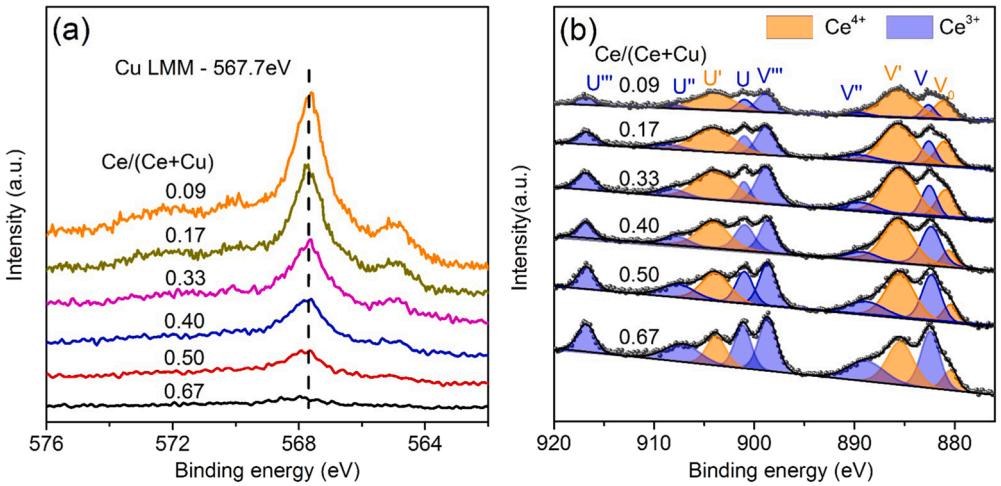

Fig. 7. (a) Cu LMM spectra and (b) Ce 3d spectra of Cu/CeO_2 catalysts with different Ce contents (Ce/(Ce+Ce) = 0.09, 017, 0.33, 0.40, 0.50, and 0.67) during $CO\text{-}H_2$ reaction (60 Pa H_2 and 5 Pa CO) at 493 K.

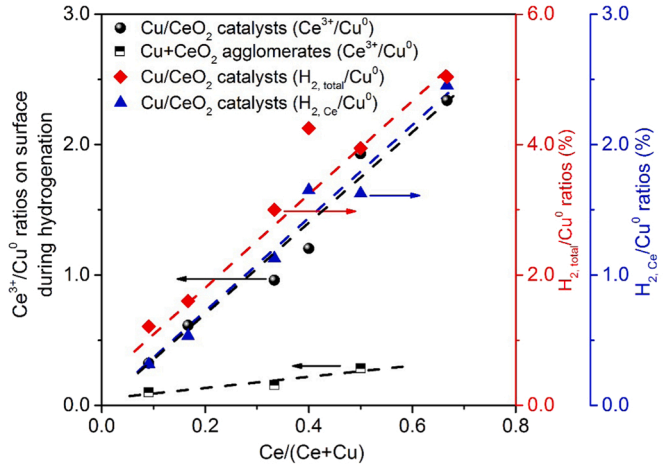

Fig. 8. The ratio of Ce^{3+}-to-Cu^0 (Ce^{3+}/Cu^0) in the surface layers of Cu-CeO_2 samples, the total irreversible H_2 uptakes ($H_{2,\ total}$, on Cu^0 and Ce^{3+} sites) and the irreversible H_2 uptakes on Ce^{3+} sites ($H_{2,\ Ce}$) normalized by the exposed metallic Cu (Cu^0) on Cu-CeO_2 samples, as functions of the Ce content in Cu-CeO_2 samples (Cu/CeO_2 catalysts and Cu+CeO_2 agglomerates) during CH_3OH synthesis.

3.4. Effects of Ce contents on the surface identities of Cu/CeO_2 catalysts

Volumetric CO uptakes were conducted to quantify the number of surface sites for CO adsorption on Cu/CeO_2 catalysts after CO hydrogenation to methanol. The CO uptakes on either monometallic Cu particles or CeO_2 were below our detection limits (1.0×10^{-8} mol). However, the CO uptakes (per surface metallic Cu atoms) at 313 K on Cu/CeO_2 catalysts, Fig. 9a, decreased from 5.9% to 4.2% with increasing Ce content in catalysts, which indicates that CO molecule might adsorb at the interfacial Cu atoms and/or interfacial CeO_2 sites in these Cu/CeO_2 catalysts. These sites may correspond to the active sites for CO activation and subsequent hydrogenation during methanol synthesis. Next, CO-DRIFTS experiments were conducted on these Cu/CeO_2 catalysts after CO hydrogenation at 493 K using CO as probe molecules, to identify the types of surface sites for CO adsorption. The pre-treated catalysts were exposed to CO at 313 K, followed by purging in Ar to remove the gas-phase CO. It is well known that the adsorption bands expected for CO stretching vibrations at above 2110 cm^{-1} and below 2100 cm^{-1} assigned to the chemisorbed CO on Cu^+ sites and metallic Cu^0 sites, respectively [74,75]. The adsorption bands for CO stretching vibrations in the ranges 2150–2178 cm^{-1} were reported previously for CO adsorbed on Ce sites [41,76,77]. None of CO adsorption band were detected on either CuO particles or CeO_2 particles at 313 K, consistent with the results of our irreversible CO uptakes. However, there is a main adsorption band for CO adsorption centered at 2098 cm^{-1} on Cu/CeO_2 catalysts (Fig. 9b), thus, the adsorption band might be assigned to the linear adsorption of CO on the metallic Cu at the interface sites of Cu-CeO_2 [75,77,78]. The CO vibrational frequencies shifted down from 2098 cm^{-1} to 2096 cm^{-1} firstly and then up to 2102 cm^{-1} with increasing the Ce content from 0.09 to 0.67, which adequately correlates with the trend of surface Ce^{3+} in Cu/CeO_2 catalysts (Fig. S18b), thus suggesting the decreasing and followed by increasing the coverages of surface oxygen (lattice oxygen) on the Cu/CeO_2 catalysts surface [77, 79].

Volumetric H_2 uptakes were also conducted to quantify the number of surface sites for the adsorption and dissociation of H_2 after CO hydrogenation to methanol on Cu/CeO_2 catalysts. The H_2 uptakes on either monometallic Cu particles or CeO_2 were below our detection limits (1.0×10^{-8} mol). Fig. 8 shows the uptakes of H_2 ($H_{2,total}/Cu^0$, per surface metallic Cu atoms) on these Cu/CeO_2 catalysts increased linearly from 1.2% to 5.0% with increasing Ce content. The trend of the variation in H_2 uptakes was consistent with that in the formation rates of methanol on these Cu/CeO_2 catalysts with increasing Ce content. Next, H_2-TPD experiments were conducted on Cu/CeO_2 catalysts after CO hydrogenation to methanol using H_2 as probe molecules, to identify the types of surface sites for H_2 adsorption and activation. On monometallic Cu particles, none of H_2 desorption peaks was detected (Fig. S19). Cu atoms bind H atoms weakly (the binding energy of H on Cu(111) fcc sites is 236 kJ mol^{-1}) [80], thus surface H* atom recombines easily with another H* and desorbs as H_2 at ambient temperature [44]. On monometallic CeO_2 particles, a negligible desorption peak appeared at about 568 K (Fig. S19), probably due to the desorption of surface hydroxyl groups [81,82]. However, addition of CeO_2 into Cu to form bimetallic particles resulted significant H_2 desorption profiles at the temperature range of 323–633 K (Fig. 10), indicating the adsorption of H_2 or dissociative adsorption of H atoms on the Cu-CeO_2 interfacial sites. Thus, the Cu-CeO_2 interfacial sites might act as active sites for CO activation and subsequent hydrogenation for methanol synthesis. We deconvoluted the H_2 desorption profiles into four desorption peaks (labeled as α, β, γ, and δ, respectively) in Fig. 10. The α and β peaks were expected for the desorption of molecular H_2 and re-combinative desorption of H atoms at the interfacial metallic Cu atoms, respectively; while γ and δ peaks could be assigned to the re-combinative desorption of H atoms at the interfacial Ce^{3+} atoms and surface reaction of hydroxy groups (OH*) on Ce species, respectively [81,83–85]. It is widely accepted that H_2 molecule adsorbs and readily dissociates on surface of transition metals (e.g. Pt,

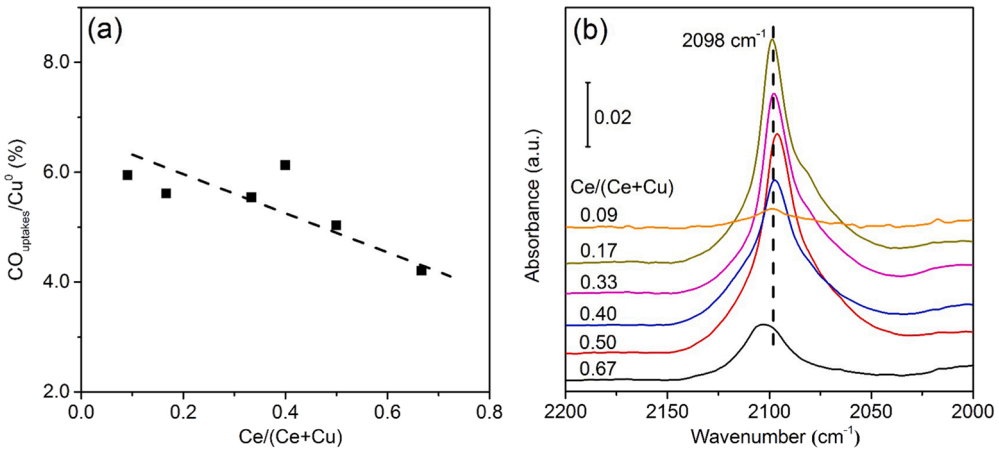

Fig. 9. (a) CO uptakes (plotted as the ratio of the amount of the adsorbed CO per exposed metallic Cu atom (Cu^0), $CO_{uptakes}/Cu^0$, Cu^0 determined from N_2O chemical titration) and (b) CO-DRIFTS on Cu/CeO_2 catalysts with different Ce contents (Ce/(Ce+Ce) = 0.09, 0.17, 0.33, 0.40, 0.50, and 0.67) at 313 K, conducted after the pretreatment in H_2 (5 kPa H_2, 100 kPa total pressure) at 503 K and then in CO-H_2 mixture (60 kPa H_2, 5 kPa CO, and 100 kPa) at 493 K.

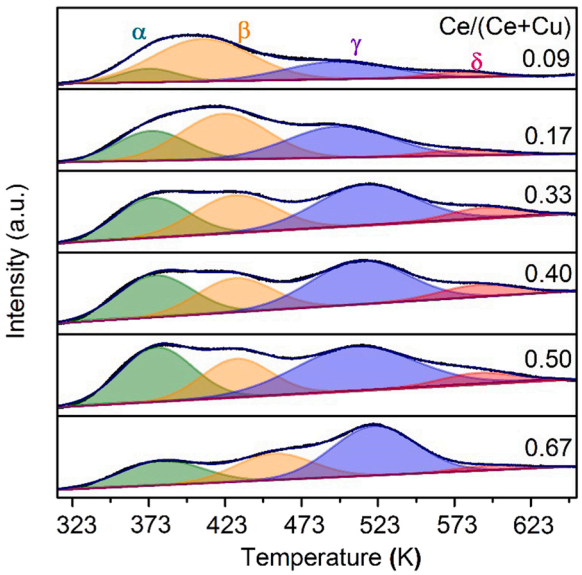

Fig. 10. H_2-TPD profiles of Cu/CeO_2 catalysts after CO hydrogenation for CH_3OH synthesis. (Ce/(Ce+Ce) = 0.09, 0.17, 0.33, 0.40, 0.50, and 0.67).

Ru and Cu clusters supported on CeO_2), subsequently migrates to an adjacent surface Ce atom through H spillover effect [20,86,87]. The temperature for H_2 desorption at Ce^{3+} atoms was apparently higher than that at metallic Cu atoms, suggesting that the Ce^{3+} atoms bind H more strongly than those of Cu atoms. All these desorption peaks shifted to higher temperature range with increasing Ce content in Cu/CeO_2 catalysts (Fig. S20a), indicates that the decoration of Ce increases the adsorption energies of H_2 and H_2 derived surface species on these sites at the interface of $Cu\text{-}CeO_2$. The fraction of H_2 adsorbed on interfacial metallic Cu sites among total H_2 uptakes gradually decreased from 69% to 48% with increasing the content of Ce (Fig. S20b), which agrees the results of CO adsorption on these interfacial Cu sites. However, the fraction of H_2 adsorbed on interfacial Ce^{3+} sites gradually increased from 26% to 49% with increasing the content of Ce (Fig. S20b), accompanied with the uptakes of H_2 on interfacial Ce^{3+} sites normalized by the exposed metallic Cu (Cu^0) ($H_{2,\ Ce}/Cu^0$, per surface metallic Ce atom) increasing linearly from 0.3% to 2.5% (Fig. 8).

3.5. Identification of the reactive surface intermediates and reaction pathway during CO hydrogenation for methanol synthesis

We next carried out the operando diffuse reflectance infrared Fourier transform spectroscopy (DRIFTS) experiments to explore the effects of Ce content on the surface reactive intermediates and the reaction pathway of methanol synthesis from $CO\text{-}H_2$ reaction on Cu/CeO_2 catalysts. Fig. 11a shows the time-resolved infrared adsorption spectra of surface reactive intermediates during methanol synthesis on Cu/CeO_2 catalysts (Ce/(Ce+Cu) ratio of 0.67), obtained after exposure to $CO\text{-}H_2$ mixture at 493 K and 100 kPa for an interval time. The infrared vibration peaks of these surface intermediates are listed in Table S4. The

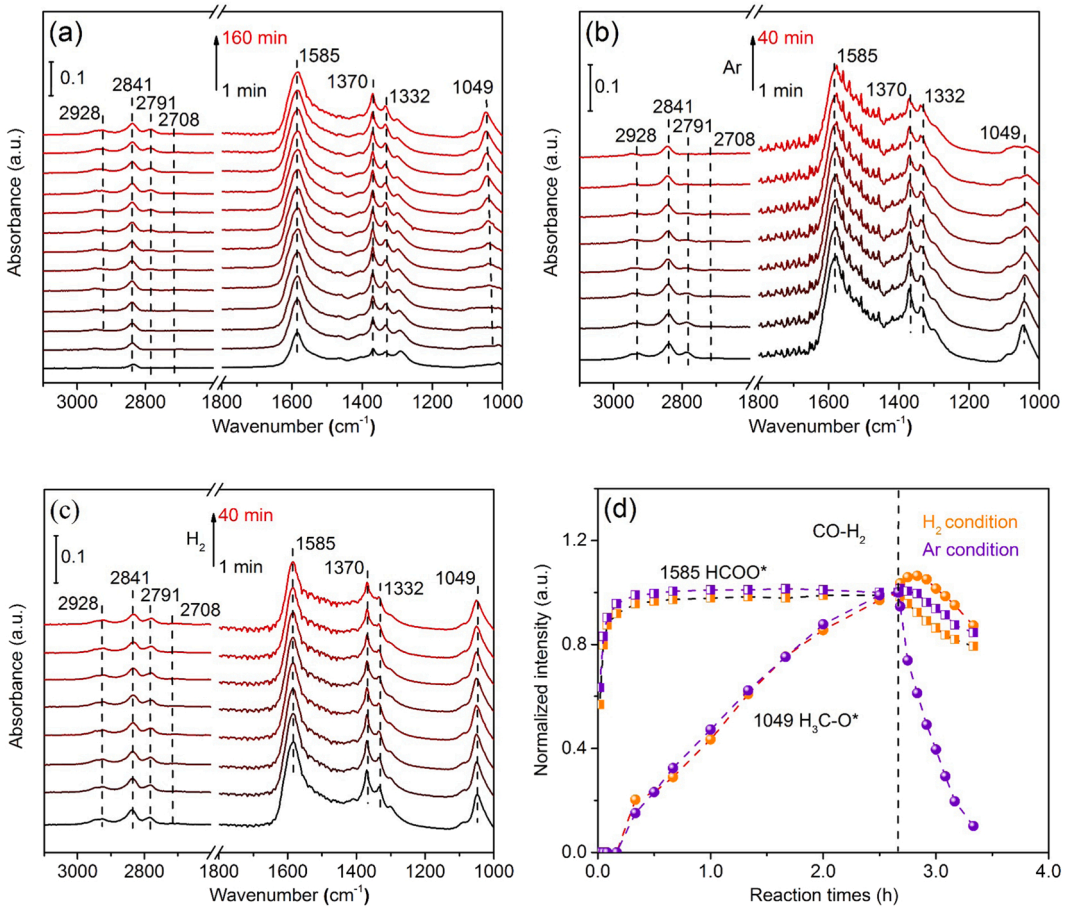

Fig. 11. (a) Operando DRIFTS spectra of Cu/CeO_2 catalyst (Ce/(Ce+Cu) = 0.67) during $CO\text{-}H_2$ reaction (60 kPa H_2 and 5 kPa CO, 100 kPa total pressure) at 493 K for about 2.6 h, followed by (b) Ar or (c) H_2 (60% H_2/Ar) treatment at 493 K for about 0.66 h. (d) Normalized intensities of major intermediate involve formate (1585 cm^{-1}) and methoxy (1049 cm^{-1}) as a function of reaction time (The intensity corresponding to formate and methoxy were normalized by the values at steady state).

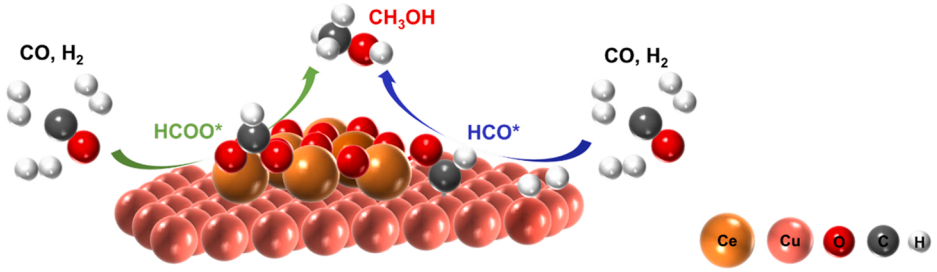

Scheme 1. Plausible mechanisms of methanol synthesis over Cu/CeO_2 catalysts.

peaks located at 1585, 1370 and 1332 cm^{-1} were expected to the asymmetric and symmetric O-C-O vibration (C═O) of the adsorbed bidentate formate species (HCOO*), while the peak centered at 2841 cm^{-1} was identified as the C-H vibration of the formate species [6,10,20,21,88]. The adsorption bands at 2928, 2791 and 1049 cm^{-1} were assigned to surface methoxy species (H_3CO*) [10,20,24,89]. The band centered at 2708 cm^{-1} was ascribed to the C-H stretching vibration in surface formyl species (HCO*) [6,21].

The vibration peaks located at 1585 and 1049 cm^{-1} were used to track the evolution of HCOO* and H_3CO* surface intermediates, respectively. HCOO* appeared immediately when Cu/CeO_2 was exposed to CO-H_2 mixture at 493 K. Its intensity gradually increased with the duration of the exposure up to 0.33 h, above which it maintained at a high, constant value (Figs. 11a, S21, S22a and S23a). The formation of HCOO* species involves a lattice oxygen atom on Cu-oxide catalysts [90] during CH_3OH synthesis from CO-H_2 reaction. Generally, CO adsorbs on a Cu site, and reacts with a nearby chemisorbed H to form HCO* at the interface of Cu-oxides [90]. The HCO* species is in a metastable state, which diffuses from the interface to the adjacent oxide surface (diffusion barrier of 0.35 eV on Cu/MgO [90]), and finally shuffles a lattice oxygen in oxide to form a formate-type species (HCO-$O_{lattice}$) [90]. In contrast, the intensity of the surface H_3CO* species raised much more slowly than those for HCOO*. It took above 2.6 h for H_3CO* species to reach their high and constant values. In addition, the intensity of CH_3OH, detected by an on-line mass spectrometry during operando DRIFTS experiments (Fig. S24), also increased slowly with the duration of the exposure. The evolution of the CH_3OH intensities adequately correlates to that of the formation of H_3CO* species on the surface of Cu/CeO_2 catalysts during CO hydrogenation to CH_3OH, indicating that the H_3CO* species could immediately react with surface H* to produce CH_3OH once the H_3CO* species formed. Therefore, the formation of surface H_3CO* species might be a kinetically relevant step for CH_3OH synthesis on Cu/CeO_2 catalysts.

Previous transient studies proposed that methanol formation occurred via the hydrogenation of HCO* intermediate during CO-H_2 reactions on Cu/CeO_2 catalysts [20,21]. The hydrogenation of HCO* route was verified by the presence of surface reactive HCO* intermediate on Cu/CeO_2 catalysts (weak adsorption peak at 2708 cm^{-1} for HCO*, Fig. 11a). However, HCOO* species, a major surface intermediates during methanol synthesis from CO-H_2 reaction, was usually recognized as a spectator [20]. In this work, transient operando DRIFTS was conducted to further explore the fate of HCOO* intermediates on these Cu/CeO_2 catalysts. The IR spectra were collected continuously at 493 K after switching the CO-H_2 mixture to either an inert gas flow (Ar) or a H_2 flow (60% H_2 in Ar) to observe the consumption of these surface intermediates. After switching to Ar, the intensities of both HCOO*and H_3CO* species coinstantaneously decayed (Fig. 11b). The HCO* species decreased immediately to a value below the experimental detection limits in pure Ar. Less than 20% H_3CO* species and 87% HCOO* species remained on Cu/CeO_2 catalysts after exposing the steady-state surface intermediates to Ar for 0.5 h. More interestingly, the intensity of HCOO* species decreased faster in H_2 than that in pure Ar (Fig. 11c), suggesting a further reductive removal of HCOO* species in presence of H_2. However, the intensity of H_3CO* species initially increased to a maximum value and then gradually decreased, indicating that the H_3CO* species accumulated immediately after exposing the surface intermediates to H_2.

These evolutions of both HCOO* and H_3CO* species suggest that H_3CO* species could also be produced via hydrogenation of surface HCOO* species (Fig. 11d). The DFT calculations show that the HCO-$O_{lattice}$ species reacts directly with a surface H* atom to form H_2CO-$O_{lattice}$ [90]. Sequential dissociation of the H_2CO-$O_{lattice}$ species lead to form H_2CO* species and release the lattice oxygen atom for its participation in the next catalytic turnover [90]. The formed H_2CO* species continues to be hydrogenated to form H_3CO* as the intermediate for CH_3OH synthesis [7,14,90]. As results, the lattice-oxygen on the Cu/CeO_2 catalysts lead the formation of HCOO* species, and opening a reaction pathway for CH_3OH synthesis from CO-H_2 mixture via the hydrogenation of HCOO* (Scheme S1). Therefore, the elementary hydrogenation steps of HCO* and HCOO* occurred concurrently on Cu/CeO_2 catalysts surface for forming surface H_3CO* species during CH_3OH synthesis from CO-H_2 mixture, but their relative contribution might differ markedly because of the difference in their coverages and activation barriers. In addition, these surface reactive intermediates on Cu/CeO_2 catalysts and their evolutions after switching the CO-H_2 mixture to either an inert gas flow (Ar) or a H_2 flow were not affected by the content of Ce in Cu/CeO_2 catalysts (Figs. 11 and S21–23). Thus, altering the Ce content did not modify the identity of the surface reactive intermediates and the reaction pathway of methanol synthesis from CO-H_2 reaction on Cu/CeO_2 catalysts.

Operando DRIFTS experiments over Cu and CeO_2 samples were carried out to further clarify the fate of these surface intermediates on Cu/CeO_2 catalysts. On the monometallic Cu particle surface, all surface intermediates and methanol were undetectable by in-situ DRIFTS and mass spectroscopy (Figs. S25 and S27a), respectively. On CeO_2 particle surface, the amount of HCOO* species gradually raised to a high and constant value under CO-H_2 reaction at 493 K for above 2.0 h (Fig. S26), while the rest of surface intermediates (e.g. H_3CO* or HCO*) were below the experimental detection limits. The bands of HCOO* adsorption shifted to higher frequencies (1595 cm^{-1}, in Table S5) on CeO_2 surface, comparing to those (1585 cm^{-1}) on Cu/CeO_2 catalysts surface (Table S4). The increase in vibrational frequency reflects a decrease in the extent of back-donation from the surface to the O-C-O orbital, which leads to stronger O-C-O bond, and in turn, suggests a weaker binding energy of HCOO* on CeO_2 surface than that on Cu/CeO_2. Although the decrease in binding energy of HCOO*, the intensity of HCOO* on CeO_2 surface remained constant after exposing the steady-state surface to H_2 (60% H_2/Ar) at 493 K. This result indicates that the subsequent hydrogenation of HCOO* to H_3CO* only occurred at the interfacial Cu-Ce sites, not on CeO_2 surface sites (Fig. S27b).

3.6. *Active sites and mechanism for methanol synthesis from CO-H_2 reaction*

Scheme 1 shows a proposed, generalized reaction pathways via surface reactive intermediates of both formyl (HCO*) [20] and formate

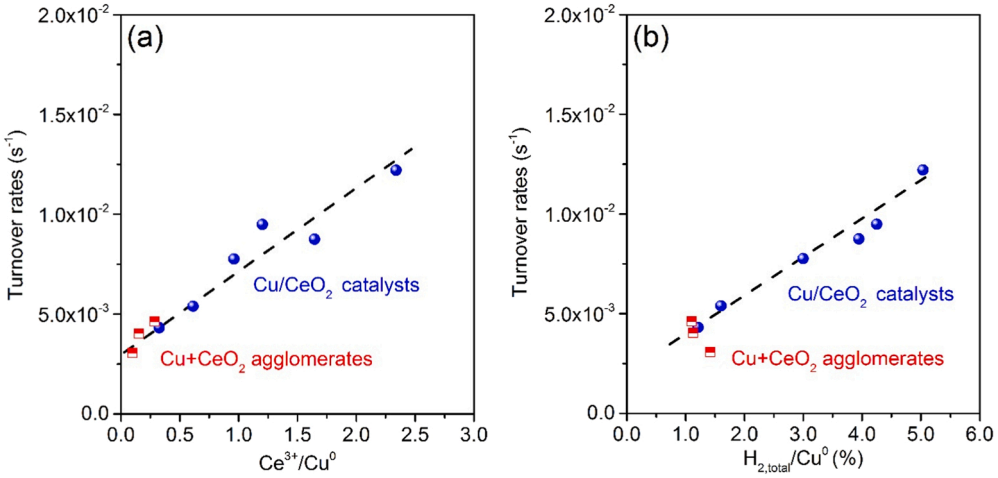

Fig. 12. Effects of (a) Ce^{3+}/Cu^0 ratio and (b) $H_{2,total}/Cu^0$ ratio on turnover rates of Cu/CeO_2 catalysts and $Cu+CeO_2$ agglomerates.

(HCOO*) for methanol synthesis from CO-H_2 reaction over Cu/CeO_2 catalysts. These two distinct reaction pathways occurred concurrently on Cu/CeO_2 catalysts surface during methanol synthesis from CO-H_2 mixture. Metallic Cu sites were proposed as active sites for the activation of H_2 [20], while the subsequent hydrogenation reaction steps, especially the reaction of HCOO* with H*, occurred at the interfacial Cu-Ce sites on the Cu/CeO_2 catalysts. We therefore quantitative analysis the relation of the intrinsic activity of Cu/CeO_2 catalysts for methanol synthesis to the interfacial Cu-Ce sites. Fig. 12 shows the turnover rates of methanol synthesis (per exposed Cu atom) as a function of the atomic ratio of Ce^{3+} to Cu^0 (Ce^{3+}/Cu^0) in the surface layers of both Cu/CeO_2 catalysts and $Cu+CeO_2$ agglomerates, and the total H_2 uptakes ($H_{2,total}/Cu^0$, per exposed Cu atom) on these Cu-CeO_2 samples (Cu/CeO_2 catalysts and $Cu+CeO_2$ agglomerates). The CH_3OH formation rates (per exposed metallic Cu atom) increased linearly with the Ce^{3+}/Cu^0 ratio on both Cu/CeO_2 catalysts and $Cu+CeO_2$ agglomerates (Fig. 12a). The linearly correlation between the turnover rates and the Ce^{3+}/Cu^0 ratio suggests that Cu^0 and Ce^{3+} sites pair may act as the active site for these subsequent hydrogenation steps for methanol synthesis. The turnover rates of methanol formation also increased linearly with the total H_2 uptakes (per exposed metallic Cu atom) on Cu/CeO_2 ($H_{2,total}/Cu^0$) (Fig. 12b), however, the rates were independent of the $H_{2,total}/Cu^0$ value on the $Cu+CeO_2$ agglomerates due to H_2 uptakes on these Cu-CeO_2 samples account for the sites of both metallic Cu atoms and Cu^0-Ce^{3+} interfacial sites.

4. Conclusions

Rate measurements, CO and H_2 uptakes/temperature-programmed desorption, and in-situ/operando spectroscopy techniques (in-situ XPS, in-situ XRD, operando DRIFTS) were used to explore the requirement of active sites and reaction pathway for CO hydrogenation to methanol over Cu/CeO_2 catalysts. The catalytic CO hydrogenation over Cu/CeO_2 catalysts formed only CH_3OH, occurring concurrently via hydrogenation of both formyl species and formate species on Cu-CeO_2 interface. Ce atoms were enriched in the surface region of Cu/CeO_2 catalysts while Ce^{3+} and Ce^{4+} atoms co-existed during CO hydrogenation. The Cu^0-Ce^{3+} sites pair acted as active sites for the direct hydrogenation of CO to methanol, its density of Cu^0-Ce^{3+} sites pair was strongly determined by the Ce content in Cu/CeO_2 catalysts and the contact extent of Cu and CeO_2 clusters. The atomic ratio of surface Ce^{3+} to Cu^0, determined by either in-situ XPS or H_2-TPD, increased linearly with increasing the content of Ce in Cu-CeO_2 samples (Cu/CeO_2 catalyst and $Cu+CeO_2$ agglomerates), thus the turnover rates of CH_3OH formation increased solely with the Ce^{3+}/Cu^0 ratio, irrespective to the contact extent between Cu and CeO_2 clusters.

CRediT authorship contribution statement

Pengchao Ren: Methodology, Investigation, Validation, Writing. **Weifeng Tu:** Conceptualization, Investigation, Writing, Funding acquisition. **Chanchan Wang:** Characterization, Investigation. **Sifan Cheng:** Synthesis, Data curation. **Wenqi Liu:** Validation. **Zhenzhou Zhang:** Data curation, Methodology. **Yun Tian:** Data curation, Investigation. **Yi-Fan Han:** Project administration, Supervision, Writing – review & editing.

Declaration of Competing Interest

The authors declare that they have no known competing financial interests or personal relationships that could have appeared to influence the work reported in this paper.

Acknowledgements

This work was financially supported by the National Natural Science Foundation of China (Grant no. 22078307, 21606208) and Henan Province Funds for Innovative Research Team in University (in Science and Technology) (18IRTSTHN001). We also acknowledge the Natural Science Foundation of Henan Province (202300410432) and the State Key Laboratory of Coal Conversion (J21-22-902).

Appendix A. Supporting information

Supplementary data associated with this article can be found in the online version at doi:10.1016/j.apcatb.2021.121016.

References

[1] G.C. Chinchen, P.J. Denny, D.G. Parker, M.S. Spencer, D.A. Whan, Mechanism of methanol synthesis from $CO_2/CO/H_2$ mixtures over copper/zinc oxide/alumina catalysts: use of ^{14}C-labelled reactants, Appl. Catal. 30 (1987) 333–338.
[2] Y. Yang, C.A. Mims, D.H. Mei, C.H.F. Peden, C.T. Campbell, Mechanistic studies of methanol synthesis over Cu from $CO/CO_2/H_2/H_2O$ mixtures: the source of C in methanol and the role of water, J. Catal. 298 (2013) 10–17.
[3] B. Yang, C. Liu, A. Halder, E.C. Tyo, A.B.F. Martinson, S. Seifert, P. Zapol, L. A. Curtiss, S. Vajda, Copper cluster size effect in methanol synthesis from CO_2, J. Phys. Chem. C 121 (2017) 10406–10412.
[4] M. Behrens, F. Studt, I. Kasatkin, S. Kuhl, M. Havecker, F. Abild-Pedersen, S. Zander, F. Girgsdies, P. Kurr, B.L. Kniep, M. Tovar, R.W. Fischer, J.K. Norskov, R. Schlogl, The active site of methanol synthesis over $Cu/ZnO/Al_2O_3$ industrial catalysts, Science 336 (2012) 893–897.
[5] S. Kuld, M. Thorhauge, H. Falsig, C.F. Elkjaer, S. Helveg, I. Chorkendorff, J. Sehested, Quantifying the promotion of Cu catalysts by ZnO for methanol synthesis, Science 352 (2016) 969–974.

[6] P. Sripada, J. Kimpton, A. Barlow, T. Williams, S. Kandasamy, S. Bhattacharya, Investigating the dynamic structural changes on Cu/CeO_2 catalysts observed during CO_2 hydrogenation, J. Catal. 381 (2020) 415–426.

[7] J. Graciani, K. Mudiyanselage, F. Xu, A.E. Baber, J. Evans, S.D. Senanayake, D. J. Stacchiola, P. Liu, J. Hrbek, J.F. Sanz, J.A. Rodriguez, Highly active copper-ceria and copper-ceria-titania catalysts for methanol synthesis from CO_2, Science 345 (2014) 546–550.

[8] F. Jiang, S. Wang, B. Liu, J. Liu, L. Wang, Y. Xiao, Y. Xu, X. Liu, Insights into the influence of CeO_2 crystal facet on CO_2 hydrogenation to methanol over Pd/CeO_2 catalysts, ACS Catal. 10 (2020) 11493–11509.

[9] A.M. Abdel-Mageed, A. Klyushin, A. Rezvani, A. Knop-Gericke, R. Schlögl, R. J. Behm, Negative charging of Au nanoparticles during methanol synthesis from CO_2/H_2 on a Au/ZnO catalyst: insights from operando IR and Near-Ambient-Pressure XPS and XAS measurements, Angew. Chem. Int. Ed. 58 (2019) 10325–10329.

[10] C. Wu, L. Lin, J. Liu, J. Zhang, F. Zhang, T. Zhou, N. Rui, S. Yao, Y. Deng, F. Yang, W. Xu, J. Luo, Y. Zhao, B. Yan, X.-D. Wen, J.A. Rodriguez, D. Ma, Inverse ZrO_2/Cu as a highly efficient methanol synthesis catalyst from CO_2 hydrogenation, Nat. Commun. 11 (2020) 5767.

[11] R.M. Palomino, P.J. Ramirez, Z.Y. Liu, R. Hamlyn, I. Waluyo, M. Mahapatra, I. Orozco, A. Hunt, J.P. Simonovis, S.D. Senanayake, J.A. Rodriguez, Hydrogenation of CO_2 on ZnO/Cu(100) and ZnO/Cu(111) catalysts: Role of copper structure and metal-oxide interface in methanol synthesis, J. Phys. Chem. B 122 (2018) 794–800.

[12] S.D. Senanayake, P.J. Ramírez, I. Waluyo, S. Kundu, K. Mudiyanselage, Z. Liu, Z. Liu, S. Axnanda, D.J. Stacchiola, J. Evans, J.A. Rodriguez, Hydrogenation of CO_2 to methanol on $CeO_x/Cu(111)$ and ZnO/Cu(111) catalysts: role of the metal–oxide interface and importance of Ce^{3+} Sites, J. Phys. Chem. C 120 (2016) 1778–1784.

[13] X.-P. Sun, F.-F. Sun, S.-Q. Gu, J. Chen, X.-L. Du, J.-Q. Wang, Y.-Y. Huang, Z. Jiang, Local structural evolutions of $CuO/ZnO/Al_2O_3$ catalyst for methanol synthesis under operando conditions studied by in situ quick X-ray absorption spectroscopy, Nucl. Sci. Tech. 28 (2016) 21.

[14] S. Kattel, P.J. Ramirez, J.G. Chen, J.A. Rodriguez, P. Liu, Active sites for CO_2 hydrogenation to methanol on Cu/ZnO catalysts, Science 355 (2017) 1296–1299.

[15] J.C. Frost, Junction effect interactions in methanol synthesis catalysts, Nature 334 (1988) 577–580.

[16] A. Tsoukalou, P.M. Abdala, D. Stoian, X. Huang, M.-G. Willinger, A. Fedorov, C. R. Müller, Structural evolution and dynamics of an In_2O_3 catalyst for CO_2 hydrogenation to methanol: an operando XAS-XRD and in Situ TEM study, J. Am. Chem. Soc. 141 (2019) 13497–13505.

[17] J. Ye, C. Liu, D. Mei, Q. Ge, Active oxygen vacancy site for methanol synthesis from CO_2 hydrogenation on $In_2O_3(110)$: a DFT study, ACS Catal. 3 (2013) 1296–1306.

[18] M.S. Frei, M. Capdevila-Cortada, R. García-Muelas, C. Mondelli, N. López, J. A. Stewart, D. Curulla Ferré, J. Pérez-Ramírez, Mechanism and microkinetics of methanol synthesis via CO_2 hydrogenation on indium oxide, J. Catal. 361 (2018) 313–321.

[19] Z. Zhang, X. Chen, J. Kang, Z. Yu, J. Tian, Z. Gong, A. Jia, R. You, K. Qian, S. He, B. Teng, Y. Cui, Y. Wang, W. Zhang, W. Huang, The active sites of Cu–ZnO catalysts for water gas shift and CO hydrogenation reactions, Nat. Commun. 12 (2021) 4331.

[20] L.G.A. van de Water, S.K. Wilkinson, R.A.P. Smith, M.J. Watson, Understanding methanol synthesis from CO/H_2 feeds over Cu/CeO_2 catalysts, J. Catal. 364 (2018) 57–68.

[21] J. Zhu, Y. Su, J. Chai, V. Muravev, N. Kosinov, E.J.M. Hensen, Mechanism and nature of active sites for methanol synthesis from CO/CO_2 on Cu/CeO_2, ACS Catal. 10 (2020) 11532–11544.

[22] J. Qu, X.W. Zhou, F. Xu, X.Q. Gong, S.C.E. Tsang, Shape effect of Pd-promoted Ga_2O_3 nanocatalysts for methanol synthesis by CO_2 hydrogenation, J. Phys. Chem. C 118 (2014) 24452–24466.

[23] X. Zhang, G. Zhang, W. Liu, F. Yuan, J. Wang, J. Zhu, X. Jiang, A. Zhang, F. Ding, C. Song, X. Guo, Reaction-driven surface reconstruction of $ZnAl_2O_4$ boosts the methanol selectivity in CO_2 catalytic hydrogenation, Appl. Catal. B: Environ. 284 (2021), 119700.

[24] J. Wang, G. Li, Z. Li, C. Tang, Z. Feng, H. An, H. Liu, T. Liu, C. Li, A highly selective and stable $ZnO-ZrO_2$ solid solution catalyst for CO_2 hydrogenation to methanol, Sci. Adv. 3 (2017), e1701290.

[25] T.P. Araújo, A. Shah, C. Mondelli, J.A. Stewart, D. Curulla Ferré, J. Pérez-Ramírez, Impact of hybrid CO_2-CO feeds on methanol synthesis over In_2O_3-based catalysts, Appl. Catal. B: Environ. 285 (2021), 119878.

[26] J.A. Rodriguez, P. Liu, D.J. Stacchiola, S.D. Senanayake, M.G. White, J.G. Chen, Hydrogenation of CO_2 to methanol: Importance of metal–oxide and metal–carbide interfaces in the activation of CO_2, ACS Catal. 5 (2015) 6696–6706.

[27] T. Fujitani, I. Nakamura, T. Uchijima, J. Nakamura, The kinetics and mechanism of methanol synthesis by hydrogenation of CO_2 over a Zn-deposited Cu(111) surface, Surf. Sci. 383 (1997) 285–298.

[28] M. Sano, T. Adaniya, T. Fujitani, J. Nakamura, Oxidation of a Zn-deposited Cu (111) surface studied by XPS and STM, Surf. Sci. 514 (2002) 261–266.

[29] Y. Choi, K. Futagami, T. Fujitani, J. Nakamura, The difference in the active sites for CO_2 and CO hydrogenations on Cu/ZnO-based methanol synthesis catalysts, Catal. Lett. 73 (2001) 27–31.

[30] J. Nakamura, Y. Choi, T. Fujitani, On the issue of the active site and the role of ZnO in Cu/ZnO methanol synthesis catalysts, Top. Catal. 22 (2003) 277–285.

[31] M. Kurtz, J. Strunk, O. Hinrichsen, M. Muhler, K. Fink, B. Meyer, C. Wöll, Active sites on oxide surfaces: ZnO-catalyzed synthesis of methanol from CO and H_2, Angew. Chem. Int. Ed. 44 (2005) 2790–2794.

[32] W.-J. Shen, Y. Ichihashi, Y. Matsumura, Low temperature methanol synthesis from carbon monoxide and hydrogen over ceria supported copper catalyst, Appl. Catal. A: Gen. 282 (2005) 221–226.

[33] W.-J. Shen, Y. Ichihashi, Y. Matsumura, Methanol synthesis from carbon monoxide and hydrogen over ceria-supported copper catalyst prepared by a coprecipitation method, Catal. Lett. 83 (2002) 33–35.

[34] M. Konsolakis, The role of Copper–Ceria interactions in catalysis science: recent theoretical and experimental advances, Appl. Catal. B: Environ. 198 (2016) 49–66.

[35] Y.H. Wang, S. Kattel, W.G. Gao, K.Z. Li, P. Liu, J.G.G. Chen, H. Wang, Exploring the ternary interactions in Cu-ZnO-ZrO_2 catalysts for efficient CO_2 hydrogenation to methanol, Nat. Commun. 10 (2019) 1166.

[36] K. Larmier, W.-C. Liao, S. Tada, E. Lam, R. Verel, A. Bansode, A. Urakawa, A. Comas-Vives, C. Copéret, CO_2-to-methanol hydrogenation on zirconia-supported copper nanoparticles: Reaction intermediates and the role of the metal–support interface, Angew. Chem. Int. Ed. 56 (2017) 2318–2323.

[37] P. Wu, B. Yang, Significance of surface formate coverage on the reaction kinetics of methanol synthesis from CO_2 hydrogenation over Cu, ACS Catal. 7 (2017) 7187–7195.

[38] Y. Kim, T.S.B. Trung, S. Yang, S. Kim, H. Lee, Mechanism of the surface hydrogen induced conversion of CO_2 to methanol at Cu(111) step sites, ACS Catal. 6 (2016) 1037–1044.

[39] S. Kattel, B. Yan, Y. Yang, J.G. Chen, P. Liu, Optimizing binding energies of key intermediates for CO_2 hydrogenation to methanol over oxide-supported copper, J. Am. Chem. Soc. 138 (2016) 12440–12450.

[40] N.D. Nielsen, J. Thrane, A.D. Jensen, J.M. Christensen, Bifunctional synergy in CO hydrogenation to methanol with supported Cu, Catal. Lett. 150 (2020) 1427–1433.

[41] A. Chen, X. Yu, Y. Zhou, S. Miao, Y. Li, S. Kuld, J. Sehested, J. Liu, T. Aoki, S. Hong, M.F. Camellone, S. Fabris, J. Ning, C. Jin, C. Yang, A. Nefedov, C. Wöll, Y. Wang, W. Shen, Structure of the catalytically active copper–ceria interfacial perimeter, Nat. Catal. 2 (2019) 334–341.

[42] W. Tu, X. Li, R. Wang, H.S. Malhi, J. Ran, Y. Shi, Y.-F. Han, Catalytic consequences of the identity of surface reactive intermediates during direct hydrogen peroxide formation on Pd particles, J. Catal. 377 (2019) 494–506.

[43] R. van den Berg, G. Prieto, G. Korpershoek, L.I. van der Wal, A.J. van Bunningen, S. Laegsgaard-Jorgensen, P.E. de Jongh, K.P. de Jong, Structure sensitivity of Cu and CuZn catalysts relevant to industrial methanol synthesis, Nat. Commun. 7 (2016) 13057–13063.

[44] A. Le Valant, C. Comminges, C. Tisseraud, C. Canaff, L. Pinard, Y. Pouilloux, The Cu-ZnO synergy in methanol synthesis from CO_2, Part 1: origin of active site explained by experimental studies and a sphere contact quantification model on Cu + ZnO mechanical mixtures, J. Catal. 324 (2015) 41–49.

[45] W. Wang, Z. Qu, L. Song, Q. Fu, CO_2 hydrogenation to methanol over Cu/CeO_2 and Cu/ZrO_2 catalysts: tuning methanol selectivity via metal-support interaction, J. Energy Chem. 40 (2020) 22–30.

[46] N. Acerbi, S.C.E. Tsang, G. Jones, S. Golunski, P. Collier, Rationalization of interactions in precious metal/ceria catalysts using the d-band center model, Angew. Chem. Int. Ed. 52 (2013) 7737–7741.

[47] S.-C. Yang, S.H. Pang, T.P. Sulmonetti, W.-N. Su, J.-F. Lee, B.-J. Hwang, C. W. Jones, Synergy between ceria oxygen vacancies and Cu nanoparticles facilitates the catalytic conversion of CO_2 to CO under mild conditions, ACS Catal. 8 (2018) 12056–12066.

[48] B. Ouyang, W.L. Tan, B. Liu, Morphology effect of nanostructure ceria on the Cu/CeO_2 catalysts for synthesis of methanol from CO_2 hydrogenation, Catal. Commun. 95 (2017) 36–39.

[49] Y.-H. Chin, C. Buda, M. Neurock, E. Iglesia, Reactivity of chemisorbed oxygen atoms and their catalytic consequences during CH_4–O_2 catalysis on supported Pt clusters, J. Am. Chem. Soc. 133 (2011) 15958–15978.

[50] Y.-H. Chin, C. Buda, M. Neurock, E. Iglesia, Consequences of metal–oxide interconversion for C–H bond activation during CH_4 reactions on Pd catalysts, J. Am. Chem. Soc. 135 (2013) 15425–15442.

[51] H. Nie, J.Y. Howe, P.T. Lachkov, Y.-H.C. Chin, Chemical and structural dynamics of nanostructures in bimetallic Pt–Pd catalysts, their inhomogeneity, and their roles in methane oxidation, ACS Catal. 9 (2019) 5445–5461.

[52] W. Tu, M. Ghoussoub, C. Veer Singh, Y.H. Chin, Consequences of surface oxophilicity of Ni, Ni-Co, and Co clusters on methane activation, J. Am. Chem. Soc. 139 (2017) 6928–6945.

[53] W. Tu, Y.-H. Chin, Catalytic consequences of the thermodynamic activities at metal cluster surfaces and their periodic reactivity trend for methanol oxidation, Angew. Chem. Int. Ed. 53 (2014) 12148–12152.

[54] B. Wang, H. Zhang, W. Xu, X. Li, W. Wang, L. Zhang, Y. Li, Z. Peng, F. Yang, Z. Liu, Nature of active sites on Cu–CeO_2 catalysts activated by high-temperature thermal aging, ACS Catal. 10 (2020) 12385–12392.

[55] J. Pang, W. Li, Z. Cao, J. Xu, X. Li, X. Zhang, Mesoporous Cu_2O–CeO_2 composite nanospheres with enhanced catalytic activity for 4-nitrophenol reduction, Appl. Surf. Sci. 439 (2018) 420–429.

[56] S.T. Hossain, E. Azeeva, K. Zhang, E.T. Zell, D.T. Bernard, S. Balaz, R. Wang, A comparative study of CO oxidation over Cu-O-Ce solid solutions and CuO/CeO_2 nanorods catalysts, Appl. Surf. Sci. 455 (2018) 132–143.

[57] W. Shan, W. Shen, C. Li, Structural characteristics and redox behaviors of $Ce_{1-x}Cu_xO_y$ solid solutions, Chem. Mater. 15 (2003) 4761–4767.

[58] J.S. Elias, N. Artrith, M. Bugnet, L. Giordano, G.A. Botton, A.M. Kolpak, Y. Shao-Horn, Elucidating the nature of the active phase in copper/ceria catalysts for CO oxidation, ACS Catal. 6 (2016) 1675–1679.

[59] X.Q. Wang, J.A. Rodriguez, J.C. Hanson, D. Gamarra, A. Martinez-Arias, M. Fernandez-Garcia, Unusual physical and chemical properties of Cu in $Ce_{1-x}Cu_xO_2$ oxides, J. Phys. Chem. B 109 (2005) 19595–19603.

[60] Z. Wu, M. Li, J. Howe, H.M. Meyer, S.H. Overbury, Probing defect sites on CeO_2 nanocrystals with well-defined surface planes by Raman spectroscopy and O_2 adsorption, Langmuir 26 (2010) 16595–16606.
[61] Z. Li, K. Tong, R. Shi, Y. Shen, Y. Zhang, Z. Yao, J. Fan, M. Thwaites, G. Shao, Reactive plasma deposition of high quality single phase CuO thin films suitable for metal oxide solar cells, J. Alloy. Compd. 695 (2017) 3116–3123.
[62] S.-Y. Ahn, H.-S. Na, K.-W. Jeon, Y.-L. Lee, K.-J. Kim, J.-O. Shim, H.-S. Roh, Effect of Cu/CeO_2 catalyst preparation methods on their characteristics for low temperature water–gas shift reaction: A detailed study, Catal. Today 352 (2020) 166–174.
[63] M. Lykaki, E. Pachatouridou, S.A.C. Carabineiro, E. Iliopoulou, C. Andriopoulou, N. Kallithrakas-Kontos, S. Boghosian, M. Konsolakis, Ceria nanoparticles shape effects on the structural defects and surface chemistry: implications in CO oxidation by Cu/CeO_2 catalysts, Appl. Catal. B: Environ. 230 (2018) 18–28.
[64] W.-W. Wang, W.-Z. Yu, P.-P. Du, H. Xu, Z. Jin, R. Si, C. Ma, S. Shi, C.-J. Jia, C.-H. Yan, Crystal plane effect of ceria on supported copper oxide cluster catalyst for CO oxidation: Importance of metal–support interaction, ACS Catal. 7 (2017) 1313–1329.
[65] E.B. Fox, A.F. Lee, K. Wilson, C.S. Song, In-situ XPS study on the reducibility of Pd-promoted Cu/CeO_2 catalysts for the oxygen-assisted water-gas-shift reaction, Top. Catal. 49 (2008) 89–96.
[66] S. Wang, L.H. Yan, Y.S. Zhao, Y.R. Ma, G.Q. Wu, J.F. Wu, S.H. Zeng, Honeycomb porous carbon frameworks from wheat flour as supports for Cu_xO-CeO_2 monolithic catalysts, Appl. Surf. Sci. 464 (2019) 294–300.
[67] K.I. Maslakov, Y.A. Teterin, A.J. Popel, A.Y. Teterin, K.E. Ivanov, S.N. Kalmykov, V. G. Petrov, P.K. Petrov, I. Farnan, XPS study of ion irradiated and unirradiated CeO_2 bulk and thin film samples, Appl. Surf. Sci. 448 (2018) 154–162.
[68] I. Ro, Y.F. Liu, M.R. Ball, D.H.K. Jackson, J.P. Chada, C. Sener, T.F. Kuech, R. J. Madon, G.W. Huber, J.A. Dumesic, Role of the Cu-ZrO_2 interfacial sites for conversion of ethanol to ethyl acetate and synthesis of methanol from CO_2 and H_2, ACS Catal. 6 (2016) 7040–7050.
[69] M. Wang, M. Shen, X. Jin, J. Tian, M. Li, Y. Zhou, L. Zhang, Y. Li, J. Shi, Oxygen vacancy generation and stabilization in CeO_{2-x} by Cu introduction with improved CO_2 photocatalytic reduction activity, ACS Catal. 9 (2019) 4573–4581.
[70] Z. Liu, P. Lustemberg, R.A. Gutiérrez, J.J. Carey, R.M. Palomino, M. Vorokhta, D. C. Grinter, P.J. Ramírez, V. Matolín, M. Nolan, M.V. Ganduglia-Pirovano, S. D. Senanayake, J.A. Rodriguez, In situ investigation of methane dry reforming on metal/ceria(111) surfaces: metal-support interactions and C-H bond activation at low temperature, Angew. Chem. Int. Ed. 56 (2017) 13041–13046.
[71] L. Szabová, M.F. Camellone, M. Huang, V. Matolín, S. Fabris, Thermodynamic, electronic and structural properties of Cu/CeO_2 surfaces and interfaces from first-principles DFT+U calculations, J. Chem. Phys. 133 (2010), 234705.
[72] J. Graciani, A.B. Vidal, J.A. Rodriguez, J.F. Sanz, Unraveling the nature of the oxide–metal interaction in ceria-based noble metal inverse catalysts, J. Phys. Chem. C 118 (2014) 26931–26938.
[73] S.Y. Yao, W.Q. Xu, A.C. Johnston-Peck, F.Z. Zhao, Z.Y. Liu, S. Luo, S. D. Senanayake, A. Martinez-Arias, W.J. Liu, J.A. Rodriguez, Morphological effects of the nanostructured ceria support on the activity and stability of CuO/CeO_2 catalysts for the water-gas shift reaction, Phys. Chem. Chem. Phys. 16 (2014) 17183–17195.
[74] A. Dandekar, M.A. Vannice, Determination of the dispersion and surface oxidation states of supported Cu catalysts, J. Catal. 178 (1998) 621–639.
[75] A.G. Sato, D.P. Volanti, D.M. Meira, S. Damyanova, E. Longo, J.M.C. Bueno, Effect of the ZrO_2 phase on the structure and behavior of supported Cu catalysts for ethanol conversion, J. Catal. 307 (2013) 1–17.
[76] C. Yang, X. Yu, S. Heißler, A. Nefedov, S. Colussi, J. Llorca, A. Trovarelli, Y. Wang, C. Wöll, Surface faceting and reconstruction of ceria nanoparticles, Angew. Chem. Int. Ed. 56 (2017) 375–379.
[77] V. Schott, H. Oberhofer, A. Birkner, M. Xu, Y. Wang, M. Muhler, K. Reuter, C. Wöll, Chemical activity of thin oxide layers: strong interactions with the support yield a new thin-film phase of ZnO, Angew. Chem. Int. Ed. 56 (2013), 12399-12399.
[78] P. Bera, A. Hornés, A.L. Cámara, A. Martínez-Arias, DRIFTS-MS studies of preferential oxidation of CO in H_2 rich stream over $(CuO)_{0.7}(CeO_2)_{0.3}$ and $(Cu_{0.9}M_{0.1}O)_{0.7}(CeO_2)_{0.3}$ (M=Co, Zn and Sn) catalysts, Catal. Today 155 (2010) 184–191.
[79] J. Greeley, A.A. Gokhale, J. Kreuser, J.A. Dumesic, H. Topsoe, N.Y. Topsoe, M. Mavrikakis, CO vibrational frequencies on methanol synthesis catalysts: a DFT study, J. Catal. 213 (2003) 63–72.
[80] J.L. Nie, H.Y. Xiao, X.T. Zu, First-principles study of H adsorption on and absorption in Cu(111) surface, Chem. Phys. 321 (2006) 48–54.
[81] Y.X. Gao, R.T. Li, S.L. Chen, L.F. Luo, T. Cao, W.X. Huang, Morphology-dependent interplay of reduction behaviors, oxygen vacancies and hydroxyl reactivity of CeO_2 nanocrystals, Phys. Chem. Chem. Phys. 17 (2015) 31862–31871.
[82] B.H. Chen, Y.S. Ma, L.B. Ding, L.S. Xu, Z.F. Wu, Q. Yuan, W.X. Huang, Reactivity of hydroxyls and water on a CeO_2(111) thin film surface: the role of oxygen vacancy, J. Phys. Chem. C 117 (2013) 5800–5810.
[83] B. Dai, G. Zhou, S. Ge, H. Xie, Z. Jiao, G. Zhang, K. Xiong, CO_2 reverse water-gas shift reaction on mesoporous M-CeO_2 catalysts, Can. J. Chem. Eng. 95 (2017) 634–642.
[84] L. Zhang, Y. Zhang, S. Chen, Effect of promoter SiO_2, TiO_2 or SiO_2-TiO_2 on the performance of CuO-ZnO-Al_2O_3 catalyst for methanol synthesis from CO_2 hydrogenation, Appl. Catal. A: Gen. 415–416 (2012) 118–123.
[85] G. Zhou, B. Dai, H. Xie, G. Zhang, K. Xiong, X. Zheng, CeCu composite catalyst for CO synthesis by reverse water-gas shift reaction: effect of Ce/Cu mole ratio, J. CO2 Util. 21 (2017) 292–301.
[86] F. Zaera, The long and winding road to catalysis, Nature 541 (2017) 37–38.
[87] B.Y. Lin, Y. Liu, L. Heng, X.Y. Wang, J. Ni, J.X. Lin, L.L. Jiang, Morphology effect of ceria on the catalytic performances of Ru/CeO_2 catalysts for ammonia synthesis, Ind. Eng. Chem. Res. 57 (2018) 9127–9135.
[88] K. Mudiyanselage, A.E. Baber, Z. Liu, S.D. Senanayake, D.J. Stacchiola, Isolation and characterization of formates on CeO_x-Cu_yO/Cu(111), Catal. Today 240 (2015) 190–200.
[89] A. Badri, C. Binet, J.-C. Lavalley, Use of methanol as an IR molecular probe to study the surface chlorination of ceria, J. Chem. Soc., Faraday Trans. 93 (1997) 1159–1168.
[90] A. Cao, Z. Wang, H. Li, A.O. Elnabawy, J.K. Nørskov, New insights on CO and CO_2 hydrogenation for methanol synthesis: the key role of adsorbate-adsorbate interactions on Cu and the highly active MgO-Cu interface, J. Catal. 400 (2021) 325–331.